J. Fluid Mech. (1984), *vol.* 142, *pp.* 391–430
Printed in Great Britain

Stresses developed by dry cohesionless granular materials sheared in an annular shear cell

By S. B. SAVAGE AND M. SAYED
Department of Civil Engineering and Applied Mechanics, McGill University, Canada

(Received 1 February 1983 and in revised form 24 January 1984)

Experimental results obtained during rapid shearing of several dry, coarse, granular materials in an annular shear cell are described. The main purpose of the tests was to obtain information that could be used to guide the theoretical development of constitutive equations suitable for the rapid flow of cohesionless bulk solids at low stress levels. The shear-cell apparatus consists of two concentric disk assemblies mounted on a fixed shaft. Granular material was contained in an annular trough in the bottom disk and capped by a lipped annular ring on the top disk. The bottom disk can be rotated at specified rates, while the top disk is loaded vertically and is restrained from rotating by a torque arm connected to a force transducer. The apparatus was thus designed to determine the shear and normal stresses as functions of solids volume fraction and shear rate.

Tests were performed with spherical glass and polystyrene beads of nearly uniform diameters, spherical polystyrene beads having a bimodal size distribution and with angular particles of crushed walnut shells. The particles ranged from about $\frac{1}{2}$ to 2 mm in size. At the lower concentrations and high shear rates the stresses are generated primarily by collisional transfer of momentum and energy. Under these conditions, both normal and shear stresses were found to be proportional to the particle density, and the squares of the shear rate and particle diameter. At higher concentrations and lower shear rates, dry friction between particles becomes increasingly important, and the stresses are proportional to the shear rate raised to a power less than two. All tests showed strong increases in stresses with increases in solids concentrations. The ratio of shear to normal stresses showed only a weak dependence upon shear rate, but it increased with decreasing concentration. At the very highest concentrations with narrow shear gaps, finite-particle-size effects became dominant and differences in stresses of as much as an order of magnitude were observed for the same shear rate and solids concentration.

1. Introduction

There are numerous applications in the field of materials handling engineering which involve the flow of dry particulate solids at high shear rates. Such granular flows are also important in the mineral-processing and pharmaceutical industries. Examples of related flows of bulk solids that occur in a geophysical context are rock falls and loose snow avalanches (Voight 1978, 1979). One of the central issues related to all these problems is the detailed form and structure of the constitutive equations that are required for the theoretical prediction of granular flows. While theoretical work on constitutive equations is at present under active development (e.g. Ogawa, Umemura & Oshima 1980; Savage & Jeffrey 1981; Ackermann & Shen 1982; Campbell & Brennen 1982*a*, *b*; Jenkins & Savage 1983), there exist few data which

can be used to guide the development and establish the validity of such theories. The present paper describes viscometric experiments performed in an annular shear cell designed to acquire this kind of experimental information.

Annular shear cells have been used previously in the fields of soil mechanics and powder technology to determine the failure and yield behaviour of granular materials under essentially quasi-static conditions involving relatively low shear rates and small strains. Typically, these cells consist of cylindrical upper and lower portions, one or both of which contain ring-like cutouts or annular troughs to contain the granular test material. Under given normal loads, torques can be applied to the two portions to generate a shear within the sample. Since there is no limit to the strains the material can experience, these devices are ideal for the study of material behaviour under conditions of continued flow. Hvorslev (1936, 1939) was the first to design an annular shear cell for soil testing. Low-strain-rate shear cells have been developed subsequently for the purpose of obtaining information for the design of bulk-solids-handling equipment by Novosad (1964), Carr & Walker (1967/68), Scarlett & Todd (1968, 1969), Scarlett *et al.* (1969/70), Mandl, deJong & Maltha (1977) and Stephens & Bridgwater (1978*a*, *b*).

Apparently, the only devices previously designed specifically to test dry, coarse granular materials at high shear rates are those developed by Novosad (1964) and Bridgwater (1972). Although Novosad did depart from quasi-static deformation in some of his tests, he did not notice any effects of shear-rate upon measured stresses. In an effort to investigate the matter further, Bridgwater developed an annular shear cell capable of achieving higher shear rates than were possible in Novosad's apparatus. Glass and plastic granular materials of different shapes and sizes were tested. The normal stress was maintained constant for each set of tests and torques were measured for various rates of rotation of the lower half of the shear cell. The results as presented suggest only slight dependence of the stresses on the rotation or shear rate. However, increasing the rotation rate while maintaining a constant normal stress in an apparatus such as Bridgwater's will result in an expansion of the bulk, decreasing the solids concentration. Since the ratio of shear stress to normal stress is almost constant in a frictional Coulomb-type material, little shear-rate dependence can be expected to be evidenced by such a test.

If the aim is to obtain stress data analogous to that usually obtained in rheological tests of solid suspensions, then it is essential to be able to maintain the mean concentration of some fixed value when the stresses are measured as functions of shear rate. This is straightforward in tests of suspensions of solids in liquids since the volume of the mixture naturally remains constant. Because of the tendency of volumetric dilatation to occur during the shear of dry particulate solids, special care must be taken in the design of the apparatus and the testing procedure to ensure that the mean concentration is kept fixed when stresses are measured as functions of shear rate in tests of these materials. The apparatus described in the present paper was designed with this essential requirement in mind.

We shall describe experimental results obtained with this apparatus in tests on several kinds of dry particulate solids; samples of monosized spherical glass and polystyrene particles having different mean diameters, spherical polystyrene particles having a bimodal size distribution, and angular irregular particles consisting of crushed walnut shells. Measurements of shear stress and normal stress versus apparent shear rate are presented for various values of mean solids concentration. The 'dynamic-friction coefficient' k, which is the ratio of shear to normal stresses on the shearing surfaces, is presented as a function of shear rate for various solids

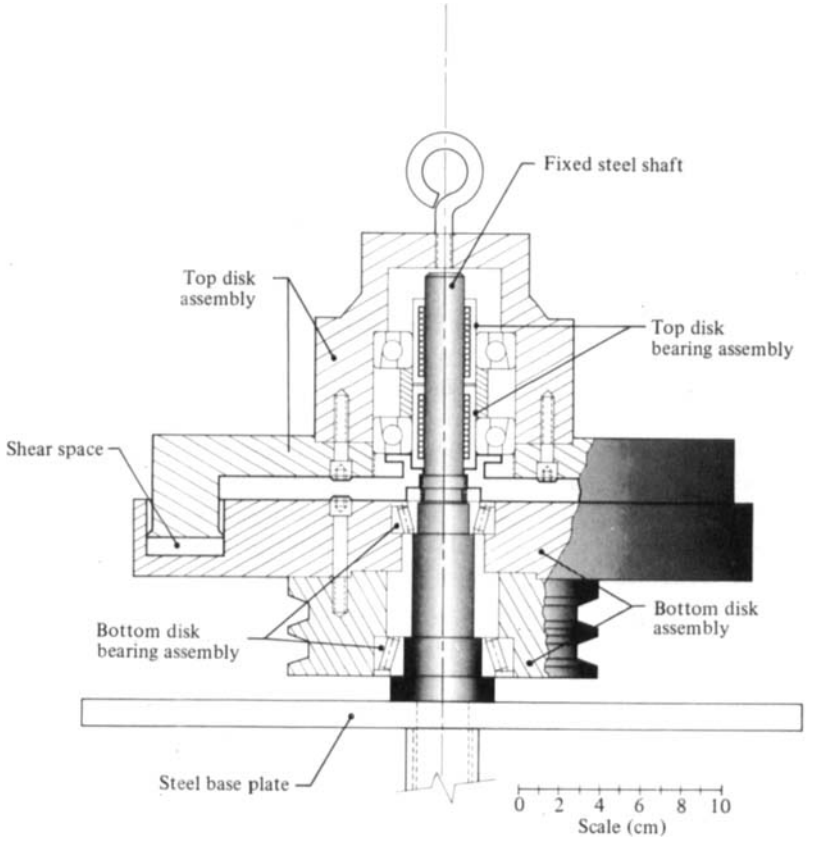

FIGURE 1. Cross-sectional view of annular shear cell.

concentrations. The various sets of data for different materials are compared with each other, and physical arguments are provided to explain the observed stress–shear-rate behaviour and a number of other unusual phenomena.

2. Experimental apparatus, procedures and test materials

2.1. *Annular shear-cell apparatus*

A cross-section of the annular shear cell used in the present tests is given in figure 1. The shear cell consists of two concentric horizontal aluminium circular disk assemblies mounted on a fixed vertical shaft. The bottom disk assembly was mounted on the shaft with two roller bearings allowing rotation but no vertical motion and was driven via a belt by a variable speed d.c. motor. This disk had an annular trough 38.1 mm wide and 28.1 mm deep on a mean radius of 127 mm. The top disk assembly was mounted on the shaft by two linear bearings and two ball bearings allowing both rotation and vertical motion. It has a lipped annular protrusion that fits in the trough in the bottom disk. This annular 'cap' was machined to close tolerances and makes no contact with the sidewalls of the trough. The top disk was restrained from rotating by a torque arm connected to a 60 g Statham load cell having a Statham Model UL4 adaptor to permit measurement of loads from 0 to 8700 g. The bottom and the top cover of the trough were lined with very coarse sandpaper having sand grains

approximately of the same size as the test particles. The purpose of the sandpaper was to prevent slipping of the particles on the surfaces that generate the shear. On the other hand, the sidewalls of the trough were finished as smoothly as possible to permit the granular material to slip there as readily as possible. The aim was to develop a nearly two-dimensional shear flow in the granular material contained between the rough upper and lower horizontal surfaces. The overall bulk density ρ and solids concentration ν (volume of solids per unit volume) were determined from a knowledge of the total mass of beads, their individual density ρ_p and the volume of the shear space. The volume of the shear space during a test run could be calculated after determining the relative positions of the upper and lower disk assemblies. The displacement of the top disk relative to the lower one was measured by Hewlett-Packard Model 7-DCDT-250 direct current differential transducer (DCDT) having a 0–12.7 mm range. The outputs of the load cell and the DCDT were recorded on a Hewlett-Packard Model 7100B two-channel recorder. The rotation rate of the bottom disk was determined by using a Texas Instrument Model TIL139 photosensor and a tape having equidistant light-reflecting spots glued around the periphery of the disk. A pulse was generated each time a spot moved by the photosensor. Knowing the spacing of the reflecting spots, the angular velocity was obtained by recording the number of output pulses in a given time interval using a Hewlett-Packard Model 5532A electronic counter. Various loads could be applied to the upper disk through a system of weights and counterweights in order to vary the applied normal and shear stresses.

2.2. *Test procedure*

The basic aim of the tests was to obtain curves of normal and shear stresses versus rates of deformation for constant values of mean solids concentration. A typical set of tests was carried out as follows. A chosen mass of particles was placed in the annular trough and then capped by the upper disk. First, counterweights were used to balance the upper disk assembly so that it was 'floating' free. Then weights were applied to the disk to develop specific normal stresses at the top of the granular material. The mass of the upper disk assembly was 15.952 kg and the applied loads ranged from 0.5 to 4.0 kg. A relatively massive upper disk assembly was chosen in an attempt to suppress vertical and rotational vibrations resulting from random stress fluctuations generated by the shear. A small initial weight was then applied and the corresponding height of the upper disk above the bottom disk (and consequently the height of the gap containing the particles) was measured using a vernier caliper. This was done to fix the zero reading of the DCDT. The torque arm of the upper disk was then connected by a horizontal string to the load cell.

Tests began by starting the drive motor and increasing the rotation rate gradually. For a given applied normal load, an increase in rotation rate increases the normal or dispersive pressures that are developed in the granular material. These dispersive stresses expand the bed of granular material and lift the upper disk assembly. The rotation rate was increased until a desired average solids concentration ν was developed. The string connecting the torque arm to the load cell was adjusted to be horizontal, and the test proceeded to obtain data to yield normal and shear stresses versus rotation rate corresponding to this particular constant value of mean ν. To do so, the loading weights and rotation rates were increased in step-like fashion. With the addition of each weight increment, the material was initially compacted and the gap height decreased; the increased shear stresses increased the torque load on the drive motor and reduced the rotation rate. The drive-motor speed and hence the shear-cell rotation rate were then increased at a constant normal load to expand the

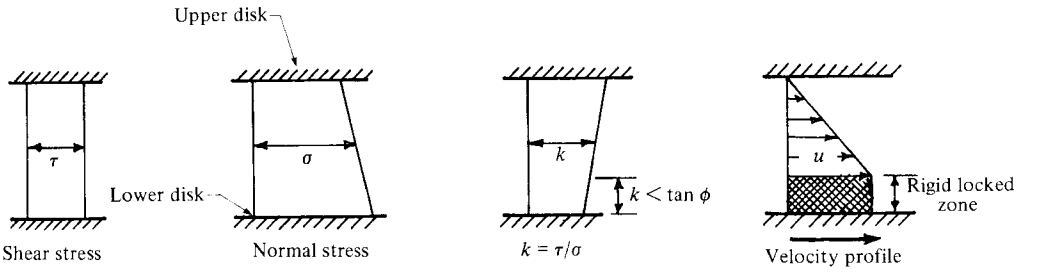

FIGURE 2. Anticipated stress and velocity distributions for case of small applied normal load, showing formation of rigid locked zone.

bed until the top disk was raised to its original level at the beginning of the test. The gap height was monitored by following the DCDT reading on the chart recorder. The normal load, torque and rotation rate corresponding to this particular test point were then recorded. Proceeding in this manner, data were obtained to yield curves of normal and shear stress versus apparent shear rate for constant values of *mean* solids concentrations. After continuing this loading sequence until some previously determined maximum load was reached, the weights and rotation rate were *decreased* in steps to return to the starting values. After each step decrease in loading weight, the gap height increased and the rotation rate had to be reduced to maintain the required gap height. The purpose of the loading–unloading sequence was to check on the reproducibility of the data or alternatively note any hysteresis effects.

The same sets of steps were repeated for several different values of ν corresponding to the different gap heights. Each series of tests for a given material began with the highest value of ν and was followed by smaller values. In some tests, ν was increased again after reaching the minimum value to check the earlier results at larger values of ν.

The maximum stresses were kept low enough to prevent particle crushing, or, in the case of polystyrene particles, to prevent the particles welding together. The minimum stresses were limited by the values needed to provide uniform shearing across the gap. At lower stresses, the particles' own weight becomes significant compared to the applied normal stress. The shear and normal-stress distributions that one might expect over the gap height for such cases are shown in figure 2. The ratio k of shear to normal stress decreases downward. If k drops to less than the value of $\tan\phi$ (where ϕ is the internal friction angle corresponding to quasi-static deformation) the material will not be sheared below this level and a rigid layer of locked particles will result. The normal stresses in the present tests ranged from 100 to 1500 N/m^2, the shear stresses from 50 to 700 N/m^2, and the shear rates from 10 to 1000 s^{-1}.

2.3. *Determination of average stresses and shear rates*

The velocity gradient and solids concentration were *assumed* to be approximately uniform over the depth and width of the trough. Thus the apparent shear rate was taken as the velocity $\bar{u}$ of the lower disk at the middle radius of the trough divided by the gap height H. Thus

$$\frac{\bar{u}}{H} = \omega(R_0 + R_i)/2H, \tag{2.1}$$

where ω is the angular velocity of the bottom disk, and R_i and R_0 are the inner and outer radii of the annular trough. Taking the apparent shear rate given by (2.1) to

be representative of the actual shear rate also assumes the no-slip condition at the rough shearing walls of the shear cell. If the collisional velocity fluctuations near the wall are small, the bulk density there is high and the wall is sufficiently rough, then it seems plausible that little slip will occur. This has been observed in some flow visualizations of other flow situations (Savage 1979). When the material is loose and the velocity fluctuations are strong, then some 'slip' at the rough wall (estimated to be of the order of the shear rate times a particle diameter) will be present.

The average solids concentration was obtained by dividing the total volume of particles by the volume of the shear space between the upper and lower disks.

The average normal stress applied to the top of the granular material is defined as

$$\sigma = \frac{N}{\pi (R_0^2 - R_1^2)}, \tag{2.2}$$

where N is the net applied weight. The torque T arising from the shear stresses developed on the upper disk is equal to the force recorded by the load cell multiplied by the radius at the torque arm. The torque is related to the local value of the shear stress $\tau_{\theta z}$ at the upper surface by

$$T = \int_{R_1}^{R_0} 2\pi r^2 \tau_{\theta z} \, \mathrm{d}r. \tag{2.3}$$

Assuming that the shear stress there is uniform, $\tau_{\theta z} = \tau$, gives

$$\tau = \frac{3}{2} \frac{T}{\pi (R_0^3 - R_1^3)}. \tag{2.4}$$

Centrifugal forces were obviously present in these experiments and caused the stresses to increase with radius. This does not affect the calculated values of the average normal stress. However, the actual average shear stress can deviate from that given by (2.4) because the effective shear force on the upper disk acts at a radius somewhat larger than the midradius of the trough as a result of the non-uniform stress distribution. An approximate analysis is presented in the Appendix to account for the centrifugal force effects on the determination of the average shear stresses. The analysis shows that these centrifugal effects are very small, reducing the average shear stresses calculated by equation (2.4) only by 1 % or 2 % for most cases. This should *not* be taken to imply that centrifugal forces are negligible, but only that their effects in the determination of the average shear stress for the present apparatus and test conditions are small. Since these particular centrifugal effects are so small and since the analysis in the Appendix is relatively crude, we have not applied the centrifugal force corrections to the data reported herein. All normal- and shear-stress data presented are based upon (2.2) and (2.4).

2.4. *Granular test materials*

Tests were performed with the following different kinds of materials.

(1) Spherical polystyrene and glass beads, each sample having a different mean diameter but a fairly uniform size distribution.

(2) Particles of crushed walnut shells to examine effects of particle angularity. These are cheap and readily available commercially. The relatively soft crushed walnut shells were chosen instead of a harder material such as sand to avoid abrasion and eventual destruction of the shear cell apparatus.

(3) Spherical polystyrene beads having a bimodal size distribution to examine the effects of strongly nonuniform particle size. These consisted of a 30–70 % mixture by

Test no.	Material	Mean diameter d (mm)	Specific gravity	Angle of internal friction ϕ	Mass of material tested M (g)	Solids concentration ν	Gap height H (mm)	Figures showing test results
PS18	I – small polystyrene beads	1.00	1.095	23°	120	0.524	6.88	8 (*a–c*)
PS19						0.504	7.15	
PS20						0.483	7.46	
PS21						0.461	7.82	
P27	II – large polystyrene beads, sample A	1.32	1.095	23°	140	0.517	8.13	9 (*a–c*)
P28						0.500	8.41	
P29						0.483	8.71	
P30						0.464	9.07	
P31						0.447	9.40	
P23	II – large polystyrene beads, sample B	1.32	1.095	23°	120	0.504	7.15	10 (*a–c*)
P24						0.483	7.46	
P25						0.461	7.82	
P26						0.443	8.15	
PS30	I – small polystyrene beads	1.00	1.095	23°	120	0.526	6.85	13
PS31					125.3	—	7.16	
PS32					131.6	—	7.51	
PS33					137.4	—	7.84	
G1	III – glass beads	1.80	2.97	25°	500	0.522	10.62	14 (*a–c*)
G2						0.507	10.92	
G3						0.491	11.28	
G4						0.477	11.61	
W11	IV – crushed walnut shells, sample A	1.19	1.177	35°	140	0.516	7.58	16 (*a–c*)
W23						0.481	8.13	
W22						0.464	8.44	
W21						0.445	8.79	
W12	IV – crushed walnut shells, sample B	1.19	1.177	35°	140	0.475	8.25	17 (*a–c*)
W13					140	0.457	8.58	
W7					115	0.446	7.21	
M1	V – mixed sizes (30% 0.55 mm and 70% 1.68 mm) polystyrene beads	1.34	1.095	24°	$M_{large}=140$	0.542	11.07	18 (*a–c*)
M2						0.528	11.38	
M3					$M_{small}=60$	0.512	11.74	
M4						0.498	12.07	

TABLE 1. Material properties and test conditions

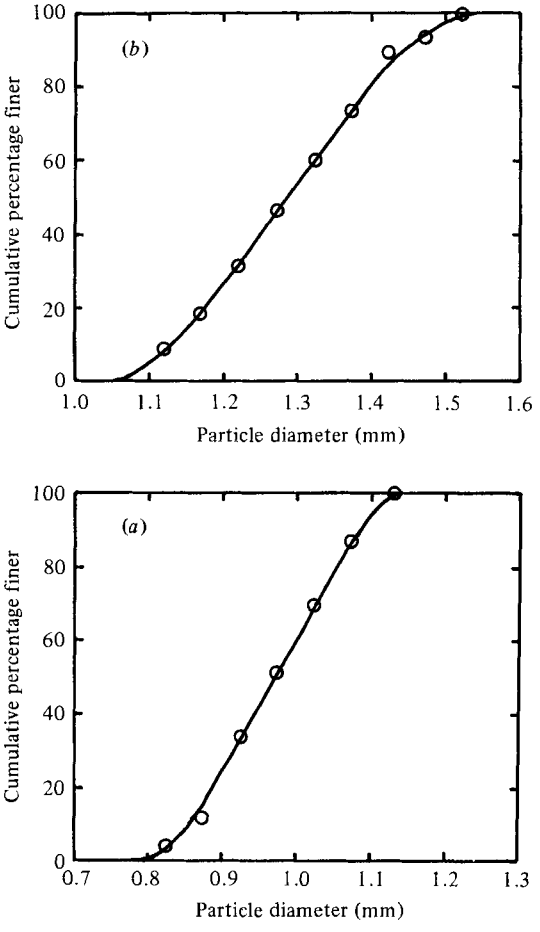

FIGURE 3. Size distributions for spherical polystyrene beads: (*a*) material I – 'small' beads; (*b*) material II – 'large' beads.

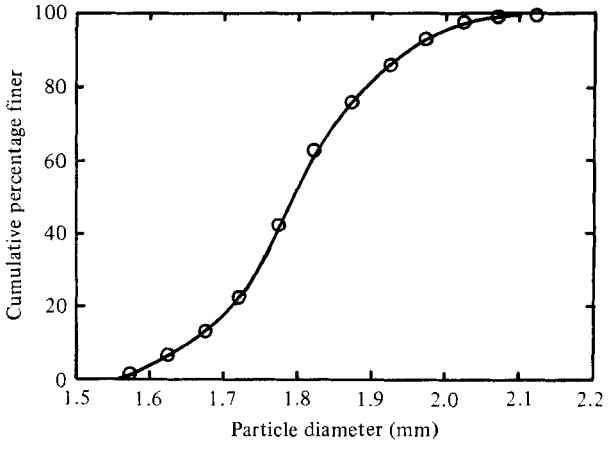

FIGURE 4. Size distribution for material III – spherical glass beads.

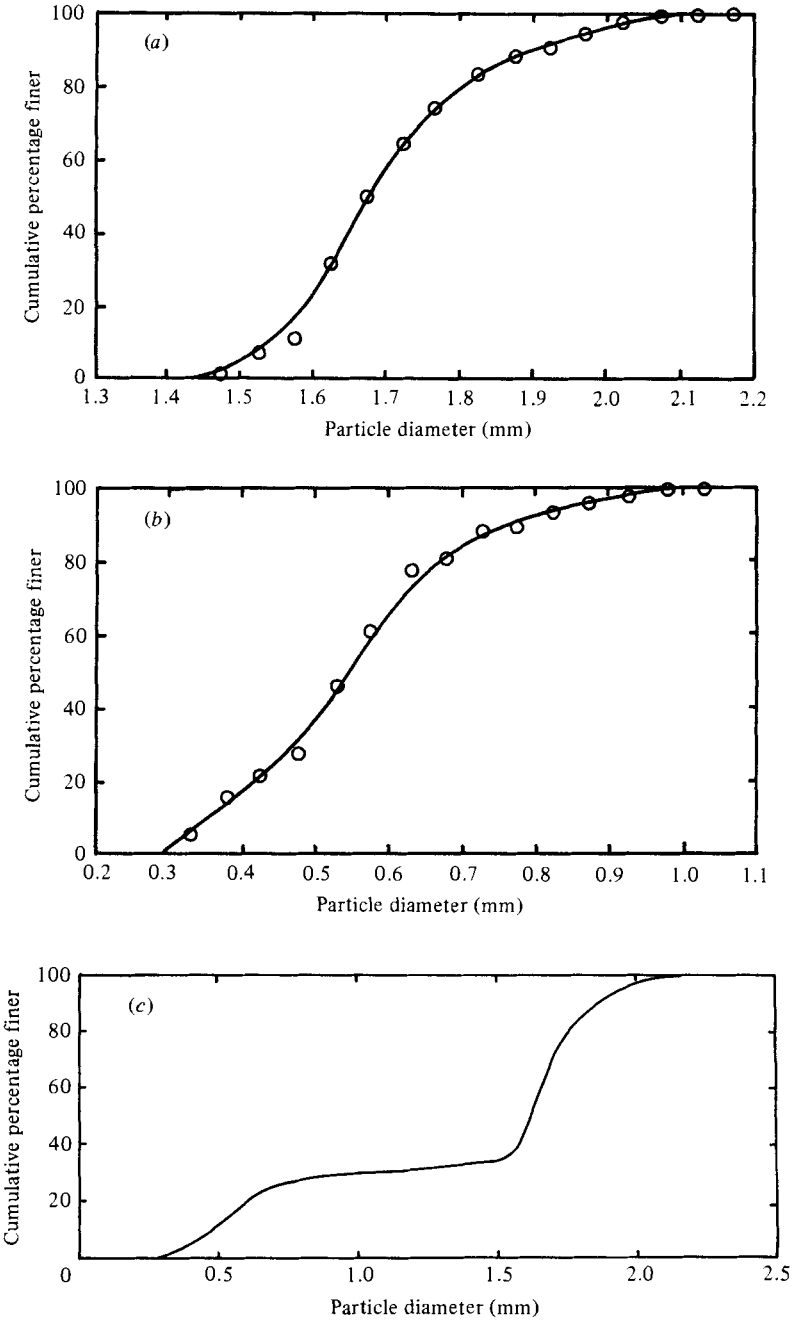

FIGURE 5. Size distributions for bimodal mixture of spherical polystyrene beads, material V: (*a*) large beads used in bimodal mixture; (*b*) small beads used in bimodal mixture; (*c*) bimodal mixture.

weight of particles of 0.55 and 1.68 mm mean diameters. The weighted mean of these two sizes is 1.34 mm.

The physical characteristics (diameters d, densities ρ_p and internal friction angles ϕ) of five different kinds of particles tested (labelled I–V) are listed in table 1. Materials I and II were spherical polystyrene beads of the same type, but somewhat

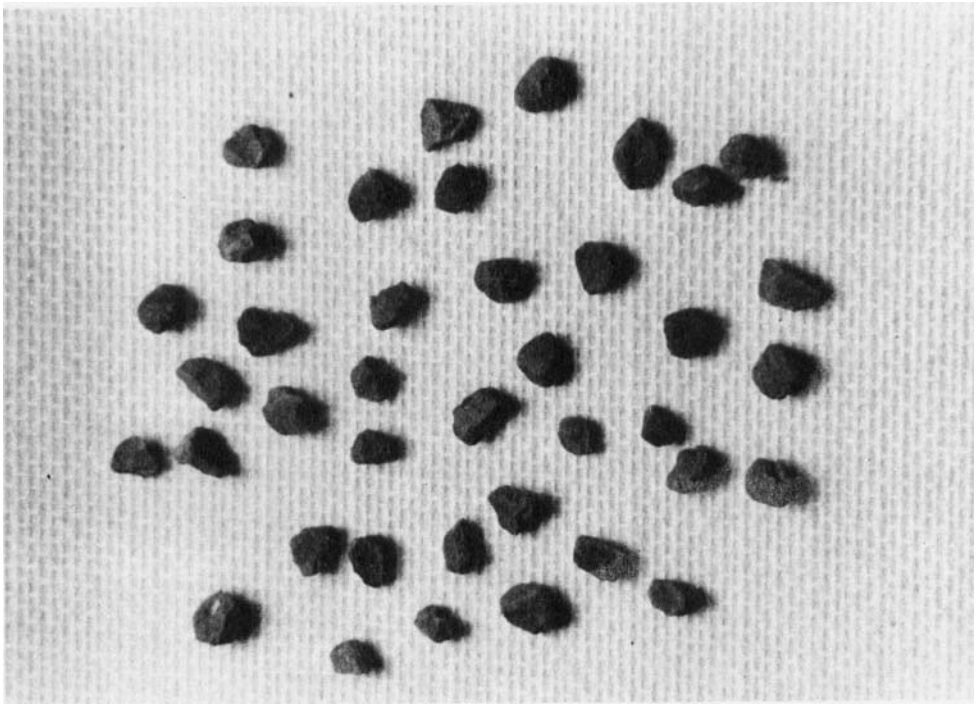

FIGURE 6. Photograph of crushed walnut shells, material IV.

different mean diameters. The two different sizes were separated from a larger batch by screening. The size distributions of the spherical particles are shown in figures 3–5. About 100 particles from each main sample were measured with a micrometer to obtain these size distributions. One may note that the *median diameters* that can be read from figures 3–5 are in some cases slightly different from the *arithmetic-mean particle diameters d* that are listed in table 1. All of the subsequent presentations of stress versus shear rate use the arithmetic mean diameters listed in table 1 to non-dimensionalize the data.

A photograph of the crushed walnut shells is shown in figure 6. The mean diameter of the crushed walnut shells was determined by the displaced-volume method using water. The quoted mean diameter of the walnut shells is the diameter of a sphere of volume equal to the average volume of an individual particle.

The angles of internal friction ϕ were determined under quasi-static conditions using a standard soil-mechanics direct-shear-test apparatus. The values of ϕ so obtained had almost the same values as the plane angles of repose for each material.

3. Preliminary experiments

A number of preliminary experiments were performed to help establish appropriate test procedures and ranges of the test variables. These tests also attempted to discover the likely reasons for some of the anomalous behaviour observed in experiments performed with the same apparatus and reported earlier by Savage (1978).

It was expected that secondary flows might develop in the granular material

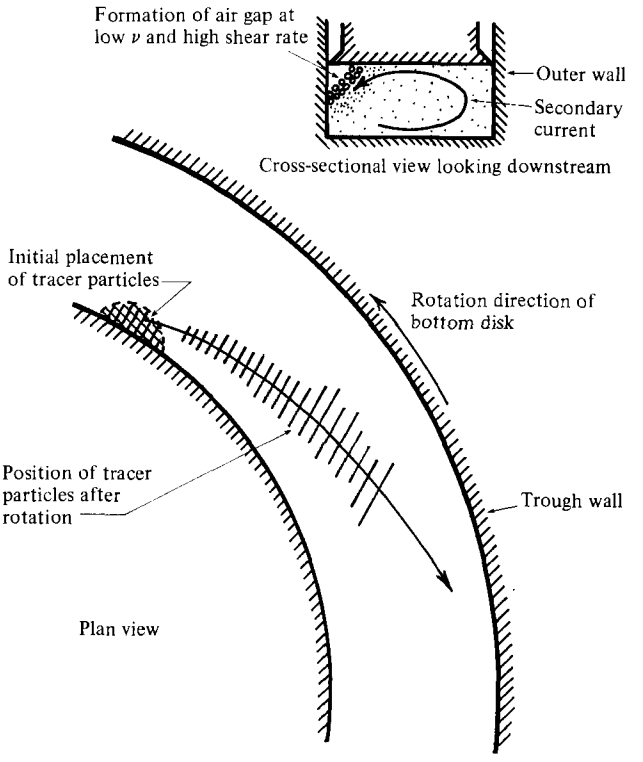

FIGURE 7. Observations of secondary flows and annular air gaps.

because of the presence of both velocity gradients and curvature in the primary flow (see Hawthorne 1965). A small amount of coloured particles was placed on the bottom of the trough adjacent to the inner wall. The trough was then filled with uncoloured particles and covered with the upper disk. After several revolutions, the test was stopped, the upper disk was taken off and the lower layers of particles were exposed by carefully sucking away the top layers with a small vacuum cleaner. As expected, the coloured particles indicated that the velocities near the bed had outward radial components as well as circumferential ones, revealing the existence of secondary currents as shown in figure 7. Although no direct measurements of such flows were made, one can infer from the directions of the tracer particles that the radial velocities associated with the secondary flows were rather smaller than the circumferential velocities. Thus, while deviations from the assumed two-dimensional simple shear flow existed, their magnitudes and their effects on the stresses are probably not too significant.

Tests were also performed to estimate the thickness of shear layers and to ensure that shear occurred over the full depth of the shear gap in order that the apparent shear rate be representative of the actual shear rate. A vertical column of coloured particles was placed among the other beads in the trough. After shearing and lifting of the top disk, layers of particles were removed carefully with a vacuum cleaner until reaching the undisturbed coloured particles. The shear depth seemed to depend on the rotation rate and the stresses, but it was roughly of the order of 10 particle diameters. This helped to establish the appropriate gap heights to be used in the experiments. Instead of employing the above procedure in every test, experiments for a given mean

ν were performed with various amounts of granular material and thus with various gap heights. Consistency of the test results when plotted in terms of stress versus shear rate was taken as an indication that the shear rate was approximately uniform over the whole depth of the flow and that no rigid flow zones existed. However, at small gap heights of less than about 5 particle diameters it was observed that the results became very inconsistent, and finite-particle-size effects became dominant. These problems are discussed in detail in §4.

It was also observed that for large rotation rates and low values of ν, the upper surface of the granular material at smaller radii could apparently lose contact with the walls and become stress-free. At the end of such tests, when the top disk was lifted, a sloped free surface adjacent to the inner wall of the trough could be seen (see figure 7). We mention that Savage (1978) reported three sets of stress–shear-rate tests at low (apparent) values of ν of 0.424, 0.456 and 0.491 which all curiously collapsed to a single curve, i.e. no dependence of stress upon concentration was evident. If a free surface formed and an essentially grain-free annular air gap developed, then the actual solids concentrations of the sheared material could have been greater than the apparent mean ν obtained by dividing the solids volume by the total volume of the shear space. If such an air gap existed in the 'low-ν' tests of Savage (1978), it is quite possible that the actual ν in the sheared material was much the same for all three tests. This could explain the *apparent* lack of any mean ν-dependence in these tests. The rotation rates employed in the present experiments were kept low enough to prevent such difficulties; this was confirmed both visually and by the consistency of the results. The analysis presented in the Appendix also gives an estimate of the normal stress at the inner wall of the trough. In the present experiments this was always positive and in most of the tests not too much less than the average normal stress. Nevertheless, the mention of such problems should emphasize that, because of the gravitational and centrifugal effects, the solids concentration is not necessarily equal to the calculated mean value but is non-uniform, highest at the lower outside radius and lowest at the upper inside radius of the annular shear gap.

In some abnormal and infrequent cases, which occured at large values of ν, the normal stresses showed only very slight dependence on the shear rate; changing the normal load at a fixed rotation rate ω had very small effect on the gap height (and consequently ν). The particles probably interlocked in such cases, forming rigid blocks in some regions inside the shear cell. In such instances, shearing would not be present over the full gap but would occur only on certain thin slip 'planes'. The forces acting on such block-like formations would be rate-independent. If most of the particles were locked together, increasing the load would have little effect on the overall solids concentration. The 'flow' would be analogous to the case of a rigid block slipping on a rough plane. This kind of behaviour was also observed in some of the results of Savage (1978) for large ν. In the present series of tests, it was found that the more usual behaviour corresponding to uniform shearing could be recovered by rapidly increasing the shear rate and slightly decreasing ν. It is likely that such a 'disturbance' broke up any 'rigid' structures of particles that could have formed.

In the tests to be reported below, we attempted insofar as was possible to avoid the 'abnormal' phenomena described above.

4. Experimental measurements and discussion

Experimental results are presented in the form of non-dimensional normal stress $\sigma/\rho_p gd$ and non-dimensional shear stress $\tau/\rho_p gd$ versus the non-dimensional apparent shear rate $\bar{u}(d/g)^{\frac{1}{2}}/H$, where σ and τ are respectively the normal and shear stress averaged over the width of the trough, ρ_p is the mass density of the individual solid grains, d is the arithmetic mean diameter, $\bar{u}$ is the linear velocity of the lower disk assembly at midtrough radius and H is the depth of granular material contained within the shear space. The material properties and test conditions are summarized in table 1.

The stresses have been made non-dimensional by dividing by the reference stress $\rho_p gd$, which is the weight per unit area of a layer of solid material one particle diameter thick. While this particular choice is not of major consequence, it does make the importance of gravitational forces for a given test point readily apparent. For tests at lower stress levels, the 'hydrostatic' stress due to the particles' own weight $\nu\rho_p gH$ can be of the same order as the stress σ applied to the upper surface of the granular material by the upper disk. Thus when $\sigma/\rho_p gd \leqslant O(\nu H/d)$ gravitational forces are significant.

When data for non-dimensional stress $\sigma/\rho_p gd$ plotted versus $\bar{u}(d/g)^{\frac{1}{2}}/H$ on log–log paper for constant values of solids concentration ν fall on a single line having a slope of two, then the physical stress σ is proportional to $\rho_p d^2(\bar{u}/H)^2$. This is consistent with the predictions of Bagnold (1954) for his *grain-inertia* regime and the more detailed microstructural theories which calculate the stresses resulting from collisional transfer of momentum and energy during nearly instantaneous collisions (e.g. Ogawa *et al.* 1980; Savage & Jeffrey 1981; Ackermann & Shen 1982; Campbell & Brennen 1982*a*, *b*; Jenkins & Savage 1983). Bagnold's (1954) simple physical argument is that the stresses in a shear flow are developed as a result of glancing collisions as the grains of one layer overtake those of an adjacent slower layer. Since both the change in momentum during a single collision and the rate at which collisions occur are proportional to the relative velocity of the two layers, the stresses are proportional to the square of the shear rate. Departures from this square shear-rate dependence may result, for example, from the effects of enduring contacts and interparticle surface friction, interparticle locking and formation of rigid zones, and significant gravitational effects.

For most of the test data, we have also presented k, the ratio of shear stress to normal stress, versus the non-dimensional shear rate $\bar{u}(d/g)^{\frac{1}{2}}/H$. This ratio k, which was determined during dynamic flow conditions, is analogous to the tangent of the internal friction angle ϕ which is commonly measured with a simple shear cell in quasi-static soil-mechanics tests.

All of the tests shown for constant values of ν (except for the single case of $H = 6.85$ mm shown in figure 13) involved at least one set of *loading* and *unloading* phases. At the lower concentrations, the measured stresses were often very nearly the same, i.e. no significant hysteresis phenomenon was observable. Thus, to avoid cluttering the graphs we have only shown data points corresponding to the mean of the loading and unloading tests in such instances. However, at high concentration, hysteresis effects were often quite noticeable and the stresses developed during both loading and unloading phases have been plotted.

A large amount of data in addition to that shown in the present paper has been obtained. The data presented herein is thought to be the more reliable of the test results and is sufficient to illustrate the main trends that were observed.

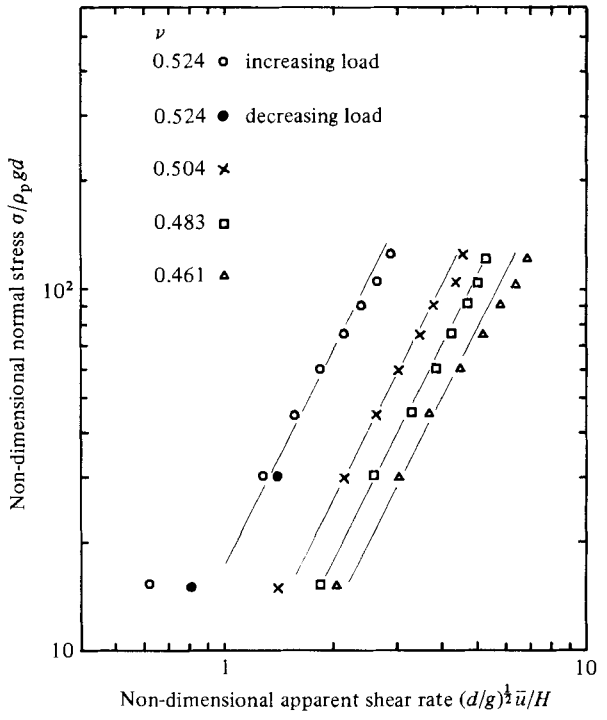

(*a*)

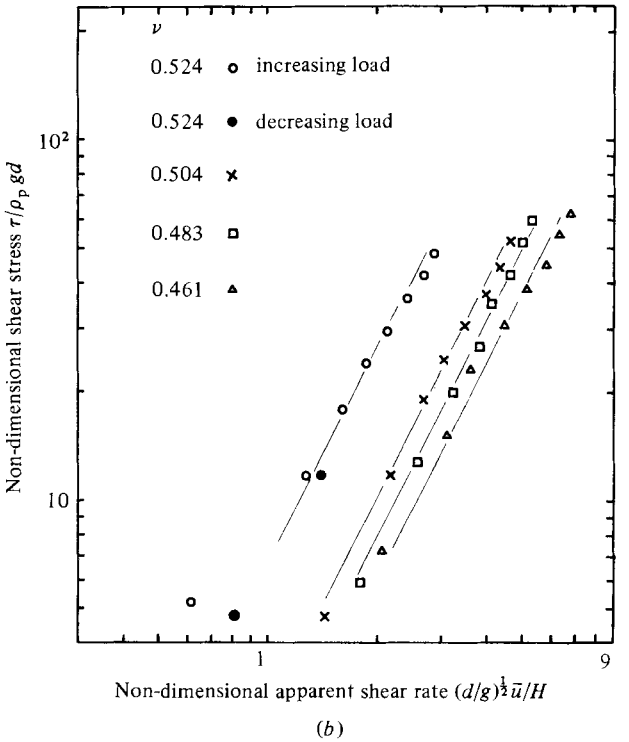

(*b*)

FIGURE 8(*a*, *b*). For caption see facing page.

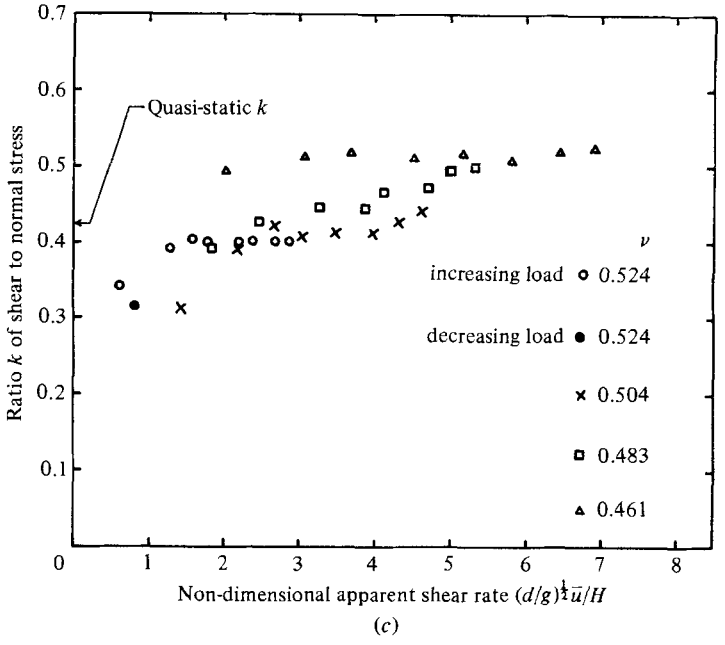

(*c*)

FIGURE 8. Experimental data for 1.0 mm mean diameter spherical polystyrene beads, material I.

4.1. *Monosized spherical beads*

4.1.1. *'Small' (1.0 mm mean diameter) polystyrene beads (material I)*

Test results for this material are shown in figures 8(*a–c*). On figure 8(*a*), showing normal stress versus apparent shear rate, we have drawn straight lines having slopes of two and arranged so as to approximately pass through the data points for constant values of solids concentration ν. At lower concentrations, the data are well represented by these straight lines, supporting Bagnold's (1954) arguments for his *grain-inertia* regime in which the stresses are developed primarily by collisional momentum transfer. A very strong increase in stresses with only small increases in solids concentraton ν is evident. At the higher concentrations and lower shear rates, the curves depart from a slope of two and tend to flatten out. This may be explained as follows. At high concentrations there is a much greater chance of enduring contacts between particles. Dry Coulomb rubbing friction during particle overriding will give rise to *rate-independent* contributions to the stresses. These contributions will be a significant fraction of the total stresses at high concentrations and low shear rates, whereas at high shear rates and low concentrations collisional momentum transfer is the dominant mechanism for stress generation. A simple superposition of the collisional contribution, which depends upon the square of the shear rate, plus the rate-independent dry friction contribution would produce the kind of curves shown.

Also evident at the highest value of $\nu = 0.524$ is a hysteresis phenomenon in which the stresses developed during the unloading phase were lower than those developed during loading. This was typical of many, but not all of the tests at high concentrations. One explanation is that, as the test progresses and material is continually sheared, the sample matures and is reworked. The particles were not perfectly uniform in size; in these tests the largest and smallest beads differed by about 30 % of the mean

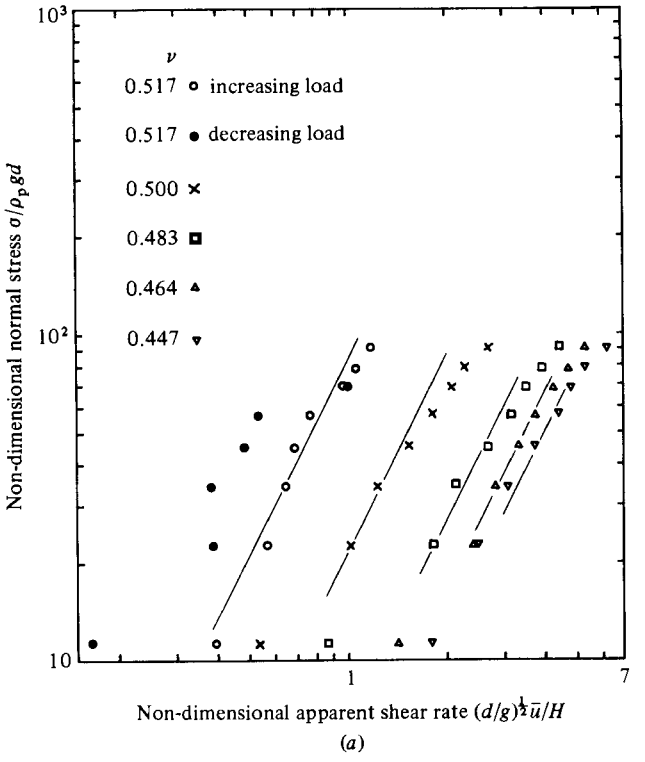

(*a*)

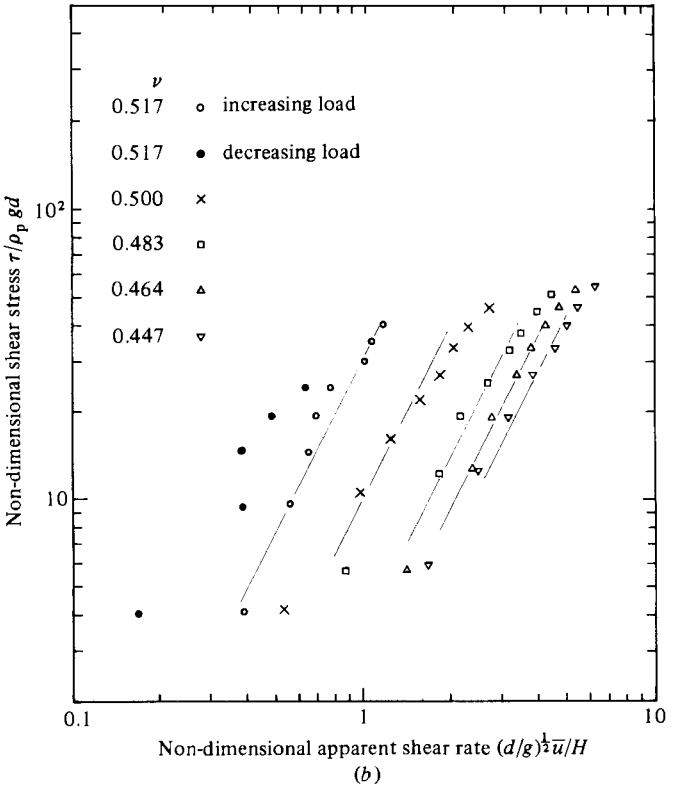

(*b*)

FIGURE 9(*a*, *b*). For caption see facing page.

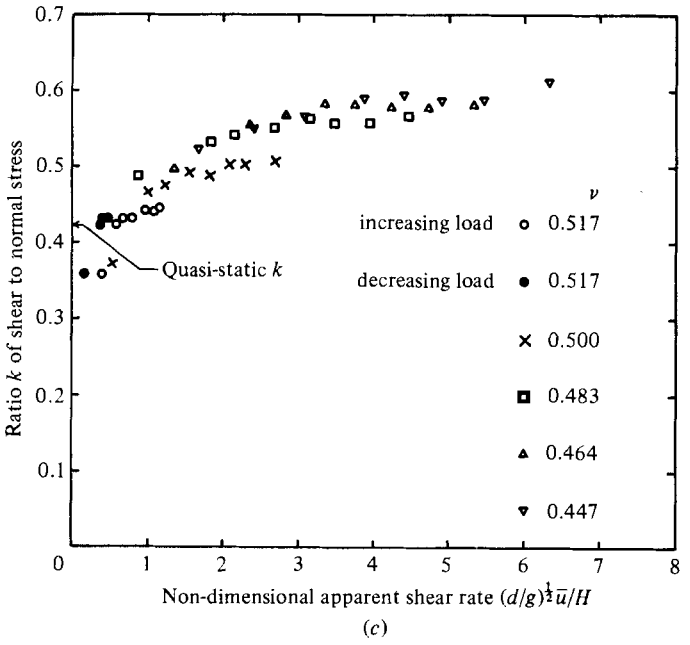

FIGURE 9. Experimental data for 1.32 mm diameter spherical polystyrene beads, material II, sample A.

diameter. While the particles may have been almost randomly mixed at the start of a test, as the test progressed the particles rearranged themselves under high stresses and placed themselves in positions and in layers so that they could most easily pass over one another during shearing with the least generation of stress. At low concentrations the collisional interactions and diffusional fluxes, combined with the secondary flows, are vigorous enough to keep the particles well mixed and hinder the ordering or 'maturing' process.

The shear stresses shown in figure 8(*b*) behave in much the same way as the normal stresses. Except at high concentrations and low shear rates, the shear stress τ is approximately proportional to $\rho_p d^2(\bar{u}/H)^2$.

Figure 8(*c*) shows the ratio of shear to normal stress versus shear rate. The quasi-static value of k corresponds to the tangent of the internal friction angle ϕ measured in the simple shear tests (table 1). The values of ϕ from the simple shear tests were essentially the same as those obtained by putting a light load on the upper disk assembly and measuring the torque when the lower disk assembly was moved very slowly by hand. As shown in figure 8(*c*) the value of k is not strongly dependent upon shear rate, but it increases slightly with decreasing concentration ν. This behaviour is *opposite* to that usually observed in *quasi-static* soil-mechanics testing at high stresses, but it is consistent with the observed gravity flows of granular materials down rough inclined planes. For steady fully developed flows, it is easily shown by integrating the linear momentum equations that the ratio of shear stress to normal stress on planes parallel to the bed must be equal to the tangent of the bed slope at all depths (Savage 1979), i.e. $k = \tan\zeta$. Experimental observations reveal that steady non-accelerating flows are possible only over a small range of values of ζ and that the solids concentration decreases with an increase in ζ. Thus the material behaviour which may be *inferred* from these inclined chute flow tests is in agreement with the shear-cell test results (figure 8*c*) obtained from direct measurements.

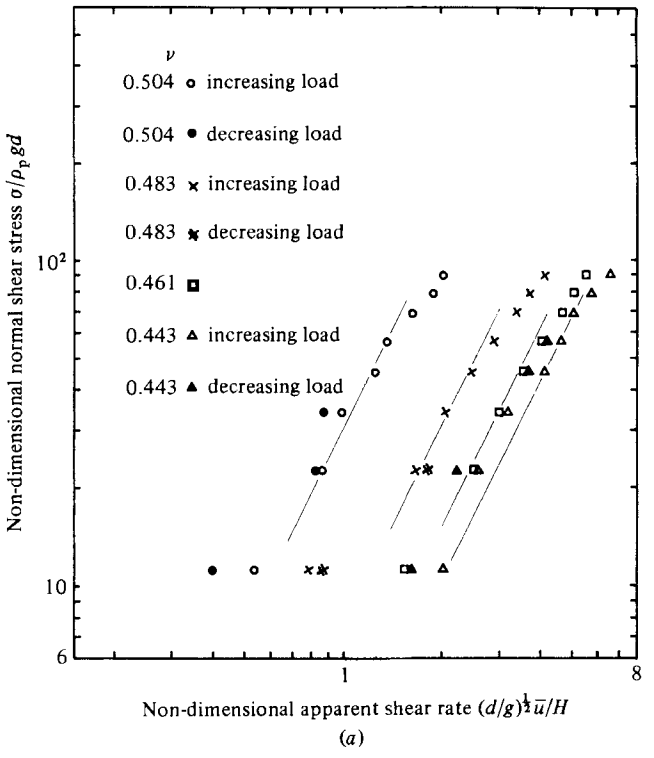

(*a*)

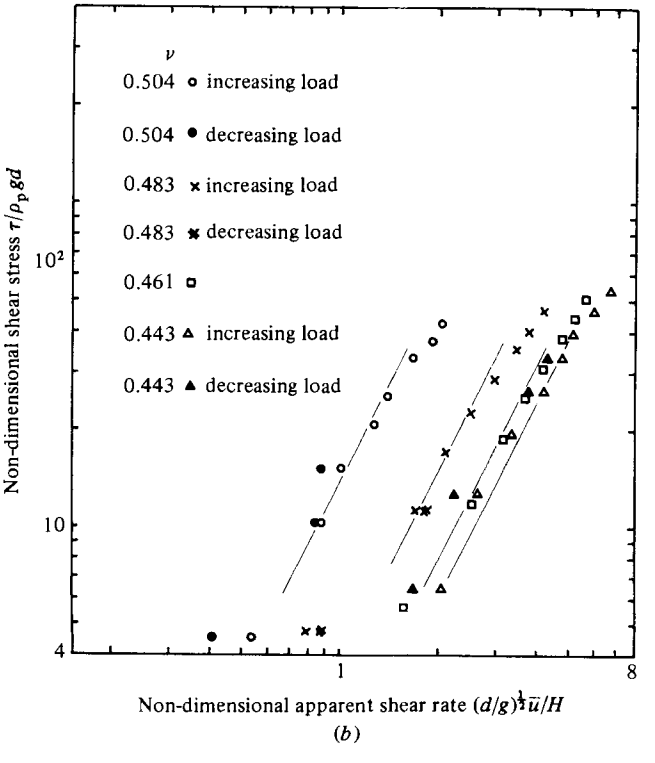

(*b*)

FIGURE 10(*a*, *b*). For caption see facing page.

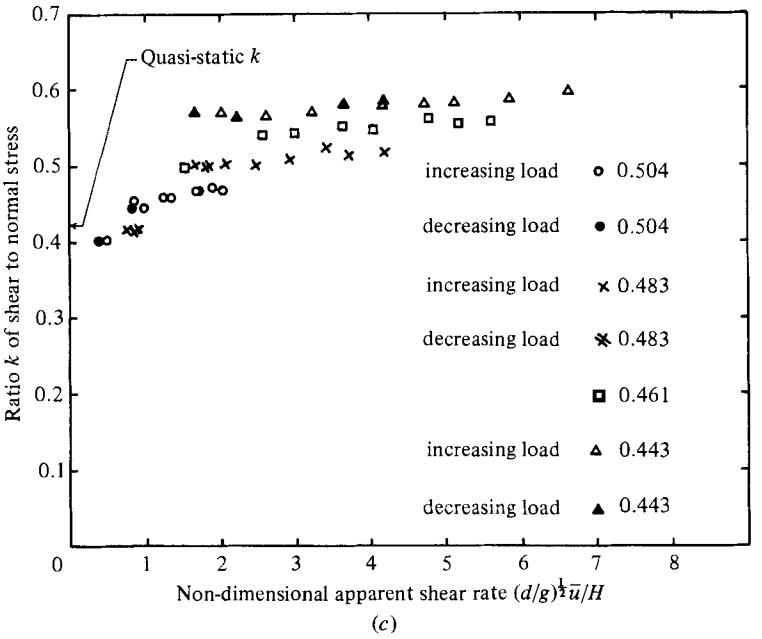

(*c*)

FIGURE 10. Experimental data for 1.32 mm mean diameter spherical polystyrene beads, material II, sample B.

A physical explanation for the difference between the dependence of k upon ν found in the present tests and that usual in quasi-static bulk solids or soil testing is as follows. The typical quasi-static test involves the initial yielding of a sample which is compacted to a fairly large concentration ν. For a given material, the larger the value of ν, the more likely is the possibility that particles are locked together in most of the sample. With the initial application of a shear load, the material must dilate in order for individual particle overrriding and shear deformation of the bulk to occur. We can expect that the shear stresses, and thus the value of k, will increase with an increase in the extent of the initial interlocking and an associated increase in the magnitude of the lateral motion involved in the particle overriding and dilatation of the bulk. Bagnold (1966) has discussed this effect in simple but more quantitative terms. More detailed discussions are found in most soil-mechanics tests (see e.g. Scott 1963). The present tests were concerned not with the initial yielding behaviour but with fully developed continuous flows. Stresses and shear rates corresponding to a set of data points were determined while the overall volume and hence the mean value of ν remained fixed. At the higher concentrations during continued shear, the particles tend to line up into distinct layers parallel to the shear surfaces. Because of the 'layering', the glancing collisions, which occur between particles in adjacent layers as one layer overtakes another, tend to be restricted to two small regions on the surface of each collision sphere which are approximately $\pm\frac{1}{2}\pi$ from the shear surfaces (which are parallel to the shearing walls of the cell). A somewhat oversimplified example of this kind of flow would be an initial simple cubic packing of spheres in which the separate layers of spheres were set into shearing motion. On the other hand, at the lower concentrations, the interstitial spaces are larger and the particle collisional velocity fluctuations are more random. Because of the larger interstitial spaces or 'holes' that are available, collisions can occur over a much larger portion of the surface of the collision sphere. These kinds of collisions are more effective in

transferring the component of momentum parallel to the shear surfaces and thus in developing shear stresses. This is suggested as a plausible explanation for the observed increase in k with decreasing ν in the present rapid shear flow experiments.

4.1.2. *'Large' (1.32 mm mean diameter) polystyrene beads (material II)*

Figures 9 and 10 show experimental results for polystyrene beads that were of the same type, but somewhat larger in diameter than those used in the tests described in the previous subsection. The present set of tests used two different samples of material II, one of 140 g and one of 120 g. The purposes were to investigate the reproducibility of data obtained from different test samples of the same material, the effect of different particle diameters and the effects of changing the shear gap height.

On figures 9 (a) and 10 (a) we have drawn straight lines having slopes of two to depict the extent to which the experimental stresses agree with the square shear-rate dependence predicted by the collisional-momentum-transfer theories. The stress data for both samples depart from these lines at the *higher stress levels* and show a somewhat weaker dependence of stress upon shear rate. The reason for this is not evident. At the higher concentrations, the stress–shear-rate curves flatten out at the lower stress levels because of the increased importance of the rate-independent stress contributions arising from dry frictional rubbing as discussed in the previous subsection.

It is interesting to note that at moderate concentrations, for example the case of $\nu = 0.483$ shown in figures 10 (a, b), the hysteresis is similar in nature to that observed for the smaller polystyrene beads (figures 8a, b). There the stresses measured during the unloading sequence were lower than those measured during loading. On the other hand, the tests for $\nu = 0.517$ shown in figures 9 (a, b) and for $\nu = 0.504$ shown in figures 10 (a, b) behave quite differently. In both these tests the stresses upon unloading are *higher* than those measured during the loading sequence. When the loads are reduced from the maximum levels reached during the loading sequence, the stresses corresponding to the unloading curve are initially almost the same as those observed during loading. Suddenly, at some critical stress or shear-rate value, there is a discontinuous change in behaviour corresponding to a jump in the 'apparent viscosity' of the shear granular material. Hoffman (1972) has observed discontinuous jumps in apparent viscosity with *increasing* shear rate in tests of concentrated ($\nu \approx 0.5$) monodisperse suspensions of PVC particles about a micron in size. On the basis of light-diffraction studies and photographs of the particle arrangements during simple shear, Hoffman proposed that the 'viscosity discontinuity' was caused by a flow instability which changed the particle arrangements from regular ordered hexagonal packings in distinct layers which could freely pass over one another to a more random packing with disordered flow and significant jamming and locking together of particles from different layers. While the mechanism for triggering the instability may be different in the present tests, it appears that the proposal of two types of flow, an ordered one in distinct layers and a more random one with intermittent particle jamming is a likely explanation of the unusual hysteresis curves observable in figures 9 (a, b) and 10 (a, b). Hysteresis curves similar to the present observations have been reported by Cheng & Richmond (1978) in connection with viscometric tests of concentrated slurries.

Figure 11 is a photograph of a typical output of the force transducer measuring the torque that the sheared granular materials applied to the upper disk assembly. The series of curves are strip-chart recordings for different loading and unloading

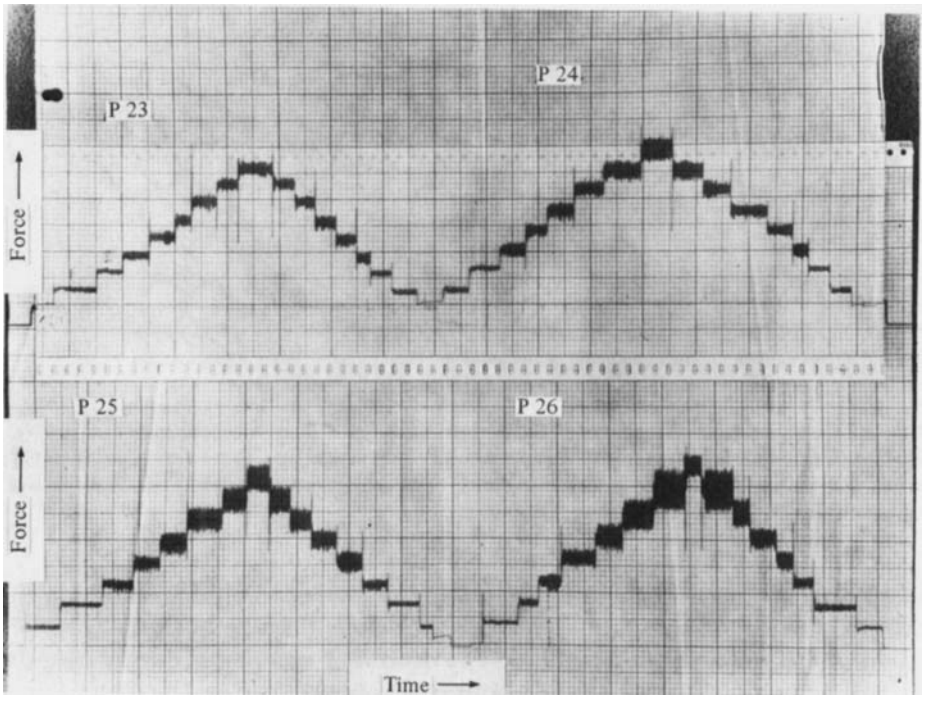

FIGURE 11. Typical strip-chart recording (tests P23–P26) of output from force transducer used to determine torque generated by sheared granular material. Fluctuations in torques increase with decreasing concentration ν.

phases for test runs P23 to P26. The widths of the bands are indications of the fluctuations in torque (or shear stress) that were present during shearing. It is interesting to note that the fluctuations were smaller at the higher concentrations (P23, $\nu = 0.504$) than at low concentrations (P26, $\nu = 0.443$) where the fluctuations in measured torque were about $\pm 15\,\%$ of the mean values. It should be noted that, because of the considerable mass of the top disk, these readings may represent the magnitudes of the torque fluctuations that are *less* than those which actually occur at the *surface of the upper-disk annular cap*.

Except for the effects described previously, the gross qualitative behaviours of the test data for large beads (figures 9 and 10) and small beads (figures 8) were quite similar. The two series of tests with the larger beads (material II, samples A and B) were consistent in that the measured stresses at a given shear rate and concentration were similar in magnitude. There were small differences in the plots of k versus non-dimensional shear rate. Tests with sample A (figure 9) gave values of k slightly higher than sample B at the low concentrations. These two series of tests were also consistent with the tests of the small beads (figure 8) at low concentrations. But, at high concentrations, the stresses measured at a given ν for the large beads were noticeably higher than those measured during shear of the small beads. This is a little surprising since all three tests used the same kind of spherical polystyrene beads. The diameter of 1.32 mm of material II was only a little larger than the 1.0 mm diameter beads of material I. One might have hoped for a collapse of all three sets of data for a given ν,

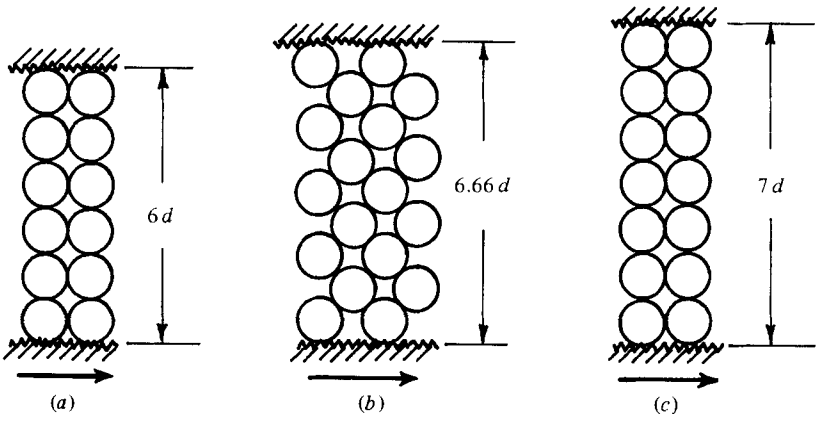

FIGURE 12. Finite-particle-size effects at high concentrations and small shear gaps: (*a*) and (*c*) show regular 'layered' shearing at concentration $\nu = 0.524$ corresponding to a sample cubic packing for shear gaps of 6 and 7 particle diameters respectively; (*b*) shows 'jammed' particles at the same concentration $\nu = 0.524$ for a shear gap of $6.66d$.

when plotted in terms of nondimensional stress versus nondimensional apparent shear rate. The only obvious difference between these three sets of tests was the ratio of gap height H to particle diameter d. The ratio H/d was largest for the test data of figure 8 showing the smallest stresses, and H/d was smallest for the data of figure 10 corresponding to the highest normal stresses. Thus finite-particle-size effects seemed a likely cause of the differences and separate tests (described in the next subsection) were performed to study them in more detail.

4.1.3. *Tests at constant ν by varying H (material I)*

Series of tests were performed in which the overall mean concentration ν was kept *constant* while the mass of material (and thus the shear gap height H) was varied from test to test. It was felt that tests of this kind, carried out at a high concentration, might yield different stresses at the same shear rate and thus reveal the significance of finite particle size effects. The sort of phenomenon that might be anticipated is shown schematically in figure 12. Consider a concentration ν a little larger than 0.524 corresponding to that of a simple cubic packing of equal spheres. If the particles arrange themselves in layers as shown, then shear can be accomplished easily (with small stresses being generated) if the gap between the rough shearing walls is an integral number of particle diameters, say 6 or 7 diameters deep as in figures 12(*a*) or (*c*) respectively. If, for example, the gap is made 6.66 diameters deep, the particles can be placed in the gap at much the same ν, by 'tilting' the simple cubic packing arrangement of figures 12(*a*, *c*) by $\frac{1}{4}\pi$. But, as is evident in figure 12(*b*), the particles now cannot be sheared but are locked together. The actual flow involving particles of slightly different sizes is bound to be rather more complicated than this figurative argument; but, if such jamming effects are present, noticeable differences in stresses should result as H is varied in steps over one particle diameter while the mean ν is kept fixed.

Figure 13 shows test data for the 1.0 mm diameter polystyrene beads (material I) in the form of non-dimensional normal stress plotted versus nondimensional apparent shear rate for various values of H. All data are for a constant mean concentration $\nu = 0.526$. The data do not collapse onto a single curve but show significant differences

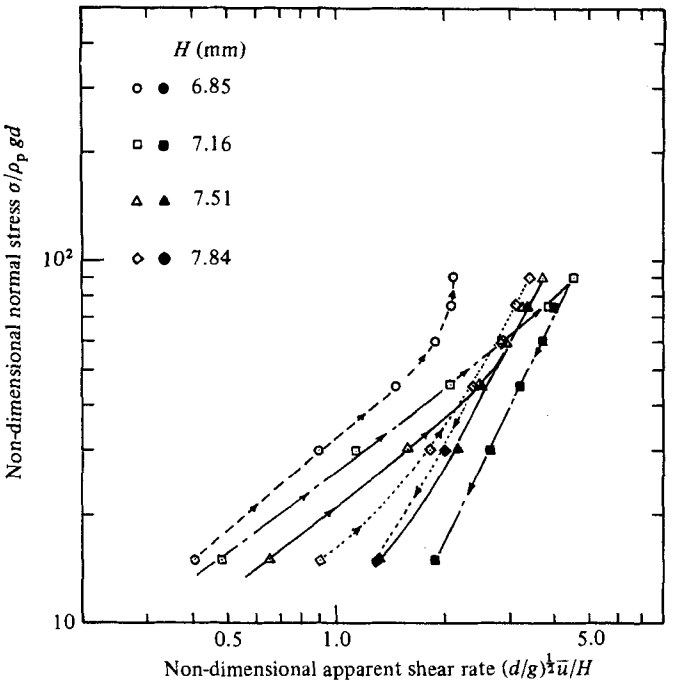

FIGURE 13. Finite-particle-size effects with 1.0 mm diameter polystyrene beads. All tests are at $\nu = 0.526$.

in stresses. In some instances the differences are almost one order of magnitude at the same value of non-dimensional shear rate. Thus, in these tests, at high concentration, finite-particle-size effects were very significant. The chronological order in which the tests for given H were performed was that of increasing H. The increment in H corresponded to the addition of a mass of beads to those already in the trough. Some of the differences in measured stresses may be due to continued reworking and ageing of material that was in the trough from the very beginning of the test series. Nevertheless, there are large differences between the individual unloading curves as well as the loading curves for different values of H. These differences can be attributed to finite-particle-size effects. Other tests performed at lower concentrations than that shown in figure 13 show a qualitatively similar, but less pronounced behaviour.

4.1.4. *Glass beads, 1.80 mm mean diameter (material III)*

Figure 14 shows data obtained using spherical glass beads as the test material. Again the stresses show a nearly square dependence upon shear rate at low concentrations. At high concentrations there is a weaker dependence at high stress levels; no doubt this is due to the increased importance of the rate-independent stress-generating mechanisms. But, at the lower stress levels at high concentrations, there is a very strong dependence upon shear rate. This increase in the slope of the stress–strain-rate curves with decreasing stress is also present (but to a much lesser extent) in the data at lower concentrations. The glass beads used in the present tests have a mass density about three times as large as that of the polystyrene beads, and gravitational forces may be responsible for the high slopes of the stress–shear-rate

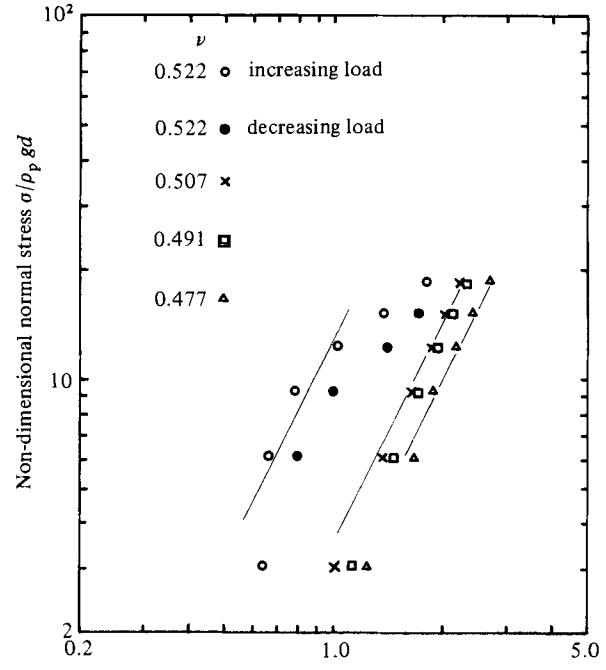

(a)

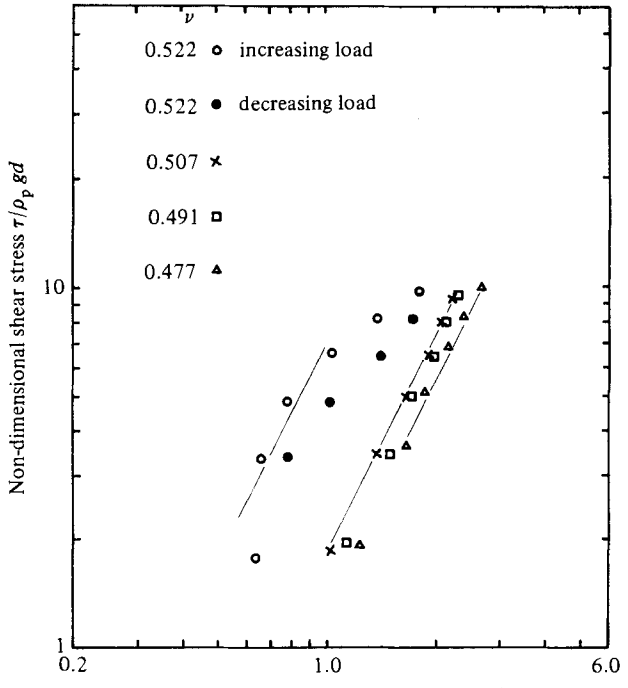

(b)

FIGURE 14(a, b). For caption see facing page.

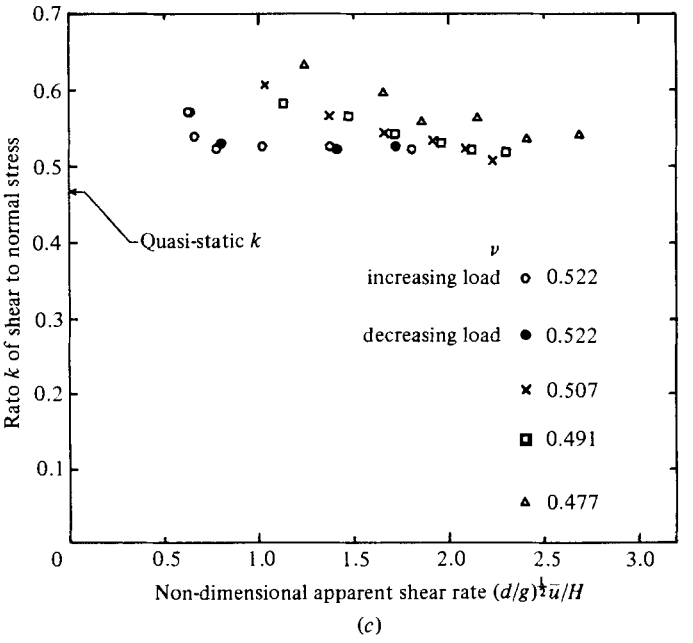

FIGURE 14. Experimental data for 1.80 mm mean diameter spherical glass beads, material III.

curves. We note that at a non-dimensional stress $\sigma/\rho_p gd = \nu H/d$ ($\nu H/d \approx 3$ in the present tests) the *change* in normal stress over the depth of the flow due to gravitational forces is the same as the stresses applied to the top of the material. At such stress levels, the normal-stress distributions depart significantly from the desired ideal of uniform values throughout the depth of material. Thus, as the applied loads (for a set of runs at constant *mean* ν) are decreased from the maximum value, gravitational forces become increasingly important. The stresses, and very likely the other quantities such as the *local* concentrations and *local* shear rate, become more and more nonuniform over the depth. Near the upper disk, where the stresses are measured, the local ν could be less than the mean value and the local shear rate higher than the apparent shear rate. If the rate at which stresses decreased as a result of lowered ν was greater than the rate at which they increased as a result of the associated increase in local shear rate, then the observed increase in slope of the stress–shear-rate curves at low stress levels may be explained. Thus, as the applied loads and shear rates are decreased, gravitational forces tend to collapse the material and hinder the collisional interactions with the upper disk. A *reduction* in shear rate which is less than that associated with a square stress–shear-rate dependence, is necessary to maintain constant H and constant mean ν.

Figures 14(a, b) show a much weaker dependence of stress upon concentration ν than was evident in the tests with the polystyrene beads. The reason for this is not clear, but it might be related to the stronger gravitational and centrifugal effects associated with the higher density glass particles. The hysteresis at high concentration in figures 14(a, b) is one in which the stresses during unloading are less than those generated during loading, indicating a reworking or maturing of the sample.

During tests with the glass beads it was observed that while the surface of the beads was smooth and polished when the sample was initially placed in the cell, by the end of a test run they acquired on opaque appearance and a roughened surface rather

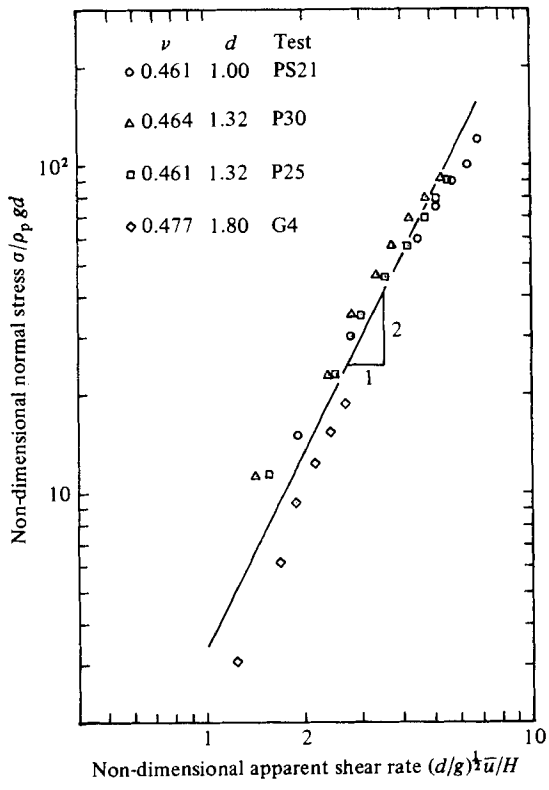

(a)

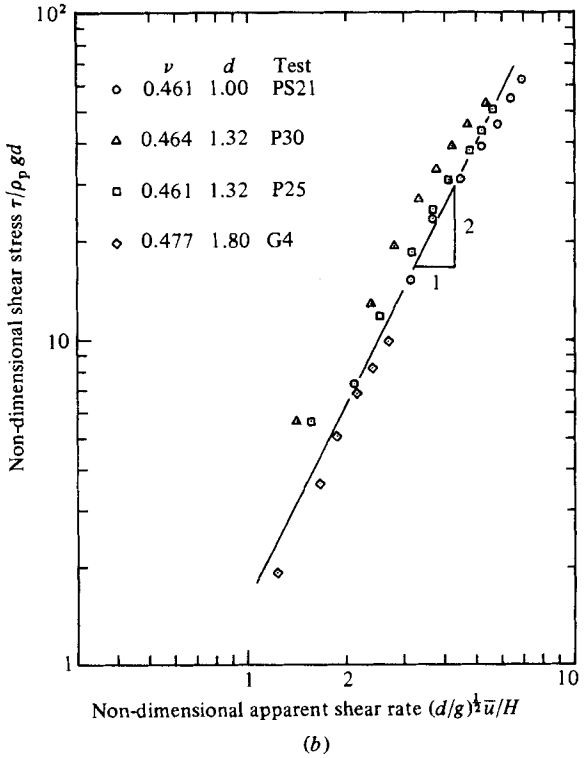

(b)

FIGURE 15(a, b). For caption see facing page.

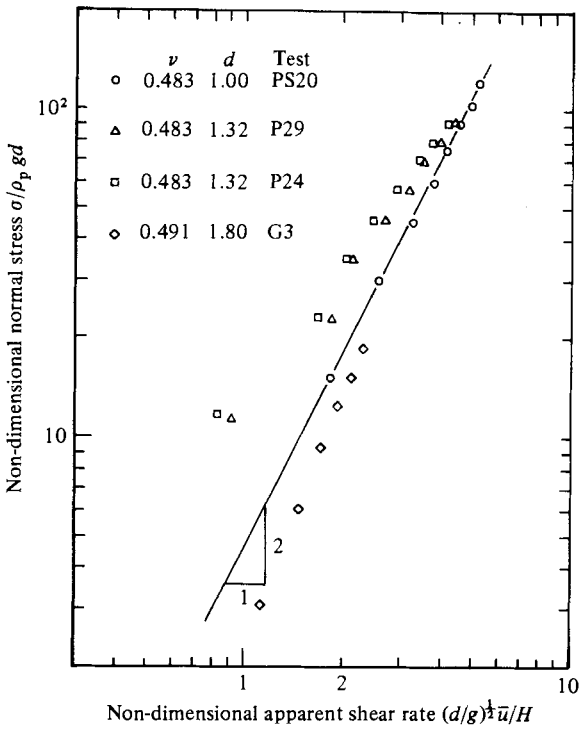

(*c*)

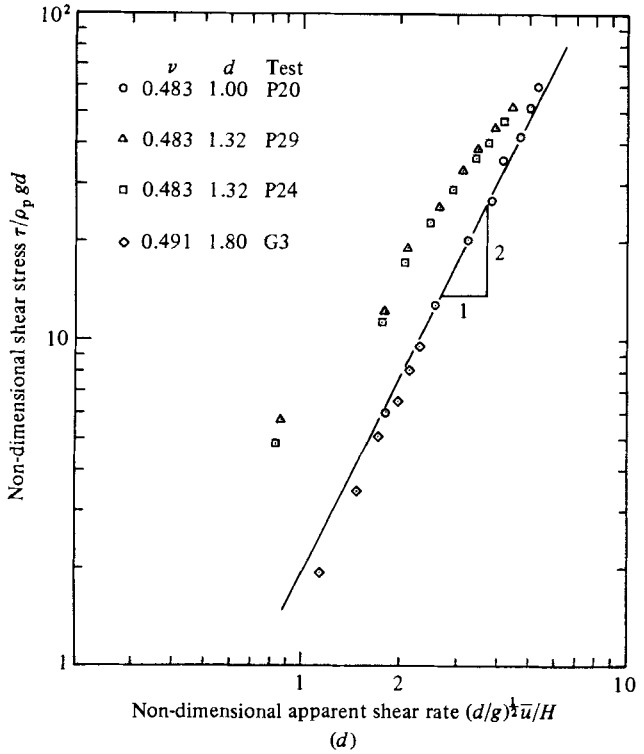

(*d*)

FIGURE 15. Comparison of experimental data obtained in tests with spherical polystyrene and glass beads: (*a*) and (*b*) are for $0.461 \leqslant \nu \leqslant 0.477$; (*c*) and (*d*) are for $0.483 \leqslant \nu \leqslant 0.491$.

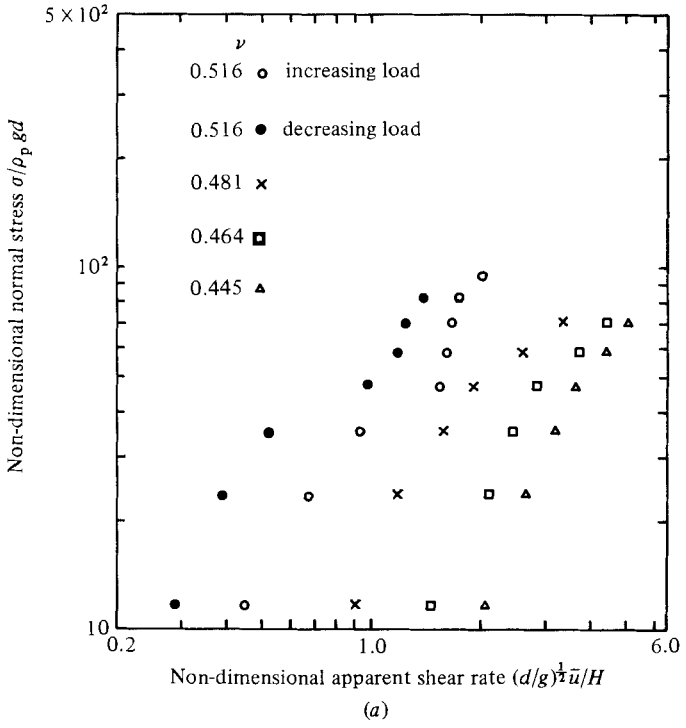

(a)

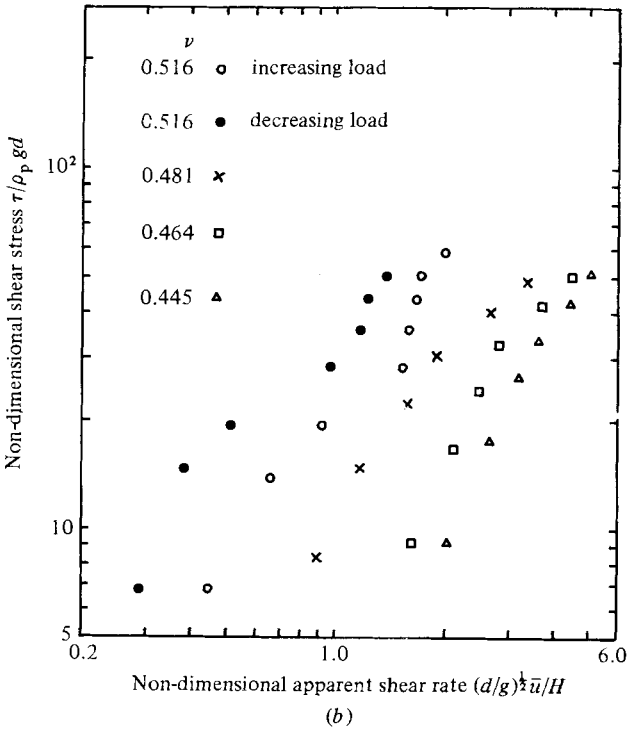

(b)

FIGURE 16(a, b). For caption see facing page.

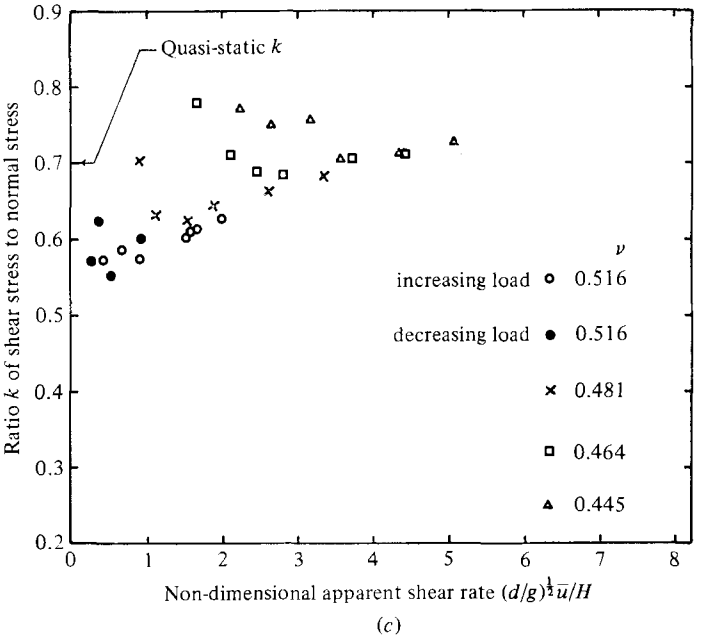

FIGURE 16. Experimental data for crushed walnut shells, material IV, sample A.

like frosted glass. Each particle suffers an enormous number of collisional impacts during a test, and the surface of the brittle glass beads becomes pitted and roughened by many tiny fractures. Small amounts of very fine powder generated by the 'grinding' of the glass beads could be found in the trough after each run. A similarly generated powder was also observed in the tests with polystyrene beads, but the amounts generated were typically less. The powder seemed to coat the plastic beads and give them a slippery feel, apparently decreasing the surface friction rather than increasing it as in the case of the glass beads.

The ratio k of shear stress to normal stress versus apparent shear rate shown in figure 14(*c*) shows a behaviour similar to that observed for the polystyrene beads in that there is an increase in k with a decrease in ν. However, the weak decrease in k with increase in shear rate is opposite to the very small increase in k with shear rate observed in most of the tests with polystyrene beads.

4.1.5. *Comparison of stress data for various spherical particles at low concentrations*

Figures 15(*a–d*) compare the stress–shear-rate data at low concentrations for the four series of tests using monosized spherical glass and polystyrene particles. Tests for the different materials were not performed at exactly the same values of ν but the comparisons are made for concentrations that are nearly the same. Figures 15(*a*, *b*) show non-dimensional shear and normal stresses versus non-dimensional apparent shear rate for values of ν of 0.461, 0.464 and 0.477. The data collapse fairly close to a line having a slope of two on these log–log plots. The data for the two tests using the large polystyrene beads are quite close to each other with the points for $\nu = 0.464$ being sightly higher than those for $\nu = 0.461$ as would be expected. The data for the small polystyrene beads tested at $\nu = 0.461$ are close to, but a little lower than, that for the larger beads at the same ν. The data for the glass beads at $\nu = 0.477$ are somewhat lower than the data for the polystyrene beads. In

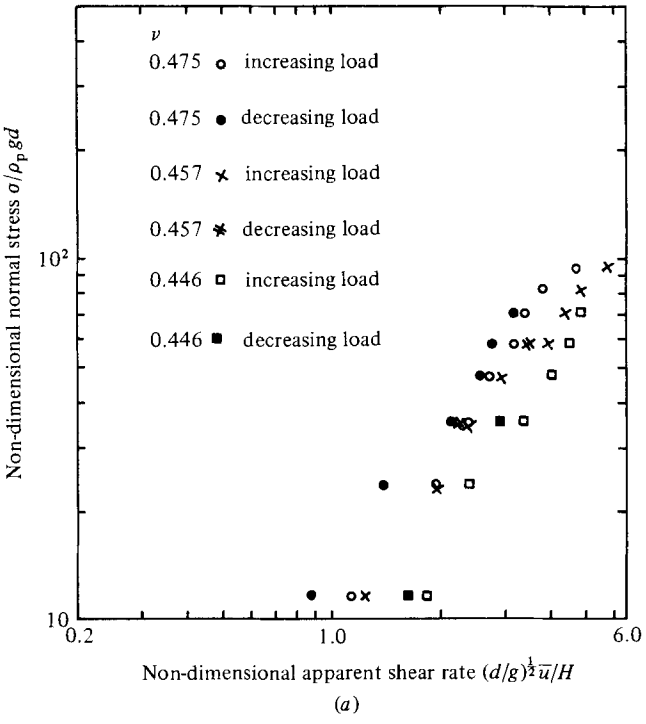

(a)

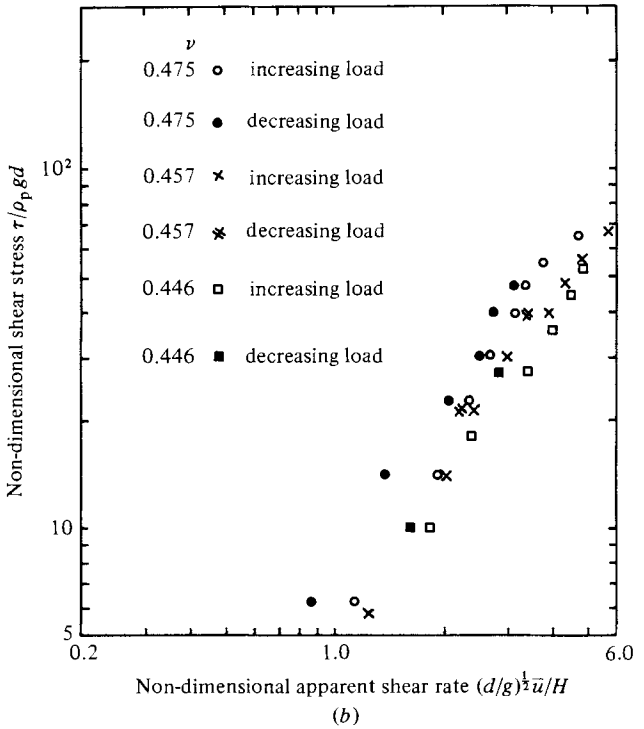

(b)

FIGURE 17 (a, b). For caption see facing page.

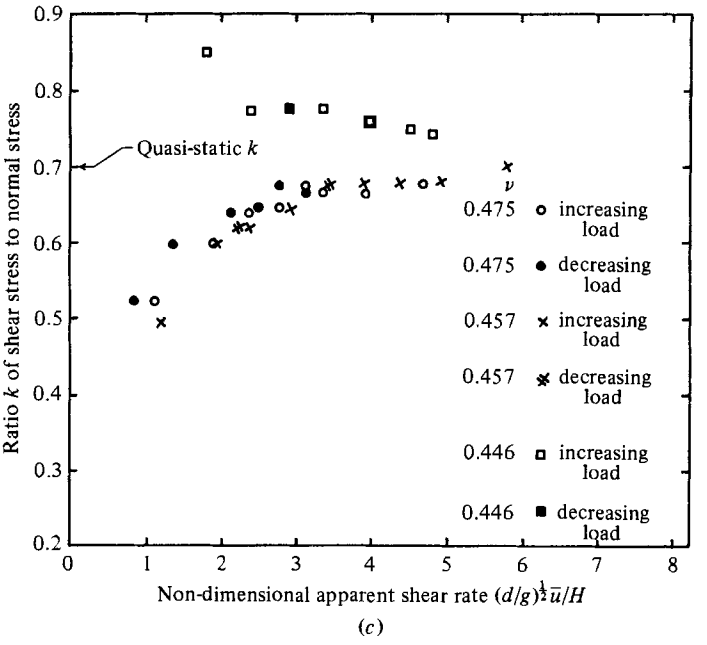

FIGURE 17. Experimental data for crushed walnut shells, material IV, sample B.

the microstructural granular-flow theories the stresses that result from collisional momentum and energy transfer depend upon the material properties of the particles. The more general analyses of Shen (1982) and Ogawa *et al.* (1980), which consider both the inelasticity and surface friction of the particles, show that the stresses *increase* with increasing coefficient of restitution e, but *decrease* with increasing coefficient of surface friction μ of the particles. Goldsmith (1968) has collected experimental data which show that e is not constant, as assumed in these theories, but varies with impact velocity. It is the highest (close to one) when the impact velocity is small and the collisions involve nearly elastic deformations, and decreases with increasing impact velocity as the plastic deformations become more significant. It appears likely that the values for e for the polystyrene beads were lower than those for the glass beads; but, as discussed previously in §4.1.4, the coefficient of surface friction μ was probably higher for the glass beads. In light of this, the lower stresses measured for the glass beads are plausible.

Figures 15(*c*, *d*) show the same kinds of data as figures 15(*a*, *b*), but they correspond to somewhat larger values of ν. The general trends are much the same as for figures 15(*a*, *b*), but the differences between the different sets of data are more noticeable. At the higher concentrations, slight differences in materials and size distributions, as well as finite-particle-size effects, significantly influence the generation of stresses.

4.2. *Particles of irregular shape, crushed walnut shells of 1.19 mm diameter (material IV)*

In order to investigate the effects that particle shape might have on the generation of stresses during shear, a number of tests were performed on crushed walnut shells (see figure 6*g*). Two sets of data are shown in figures 16 and 17. The stress–shear-rate data are quite consistent and the differences between the stresses measured using the

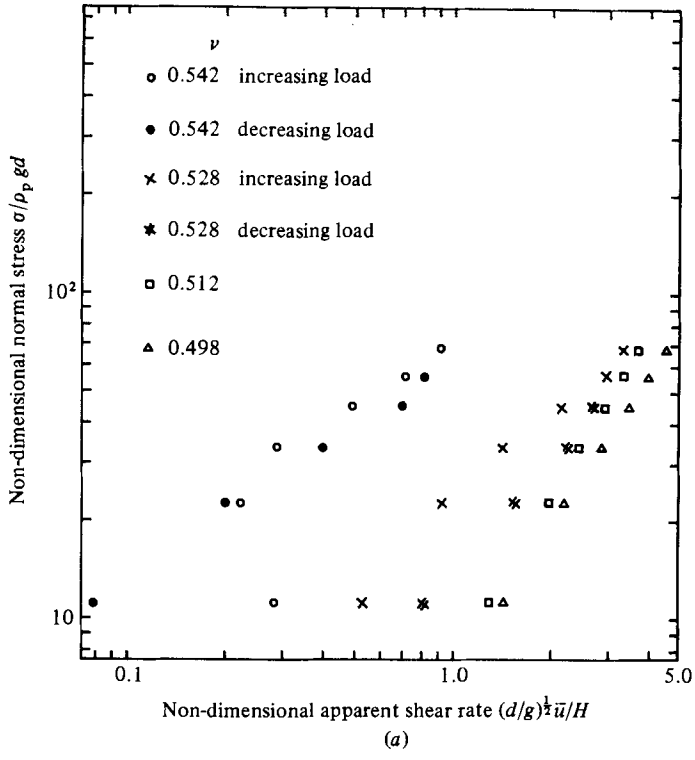

(a)

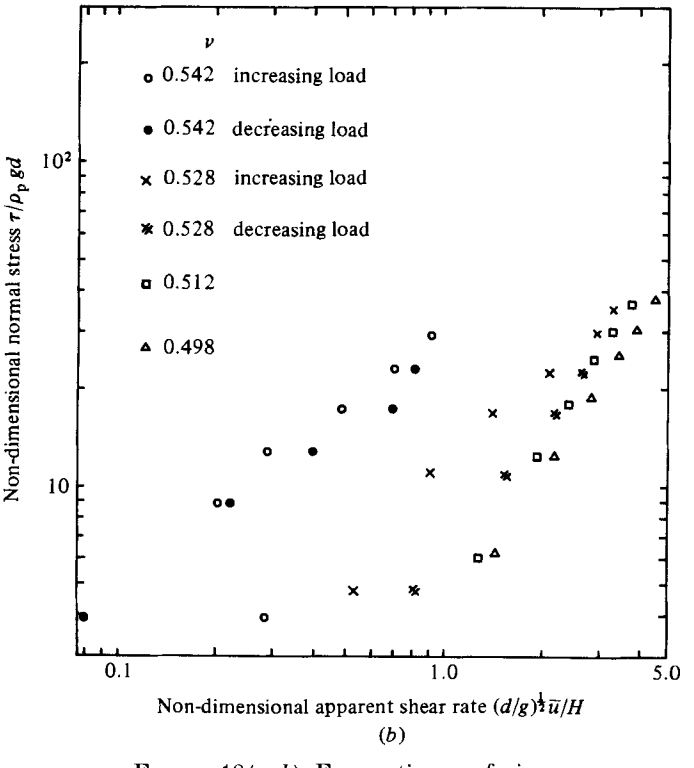

(b)

FIGURE 18(a, b). For caption see facing page.

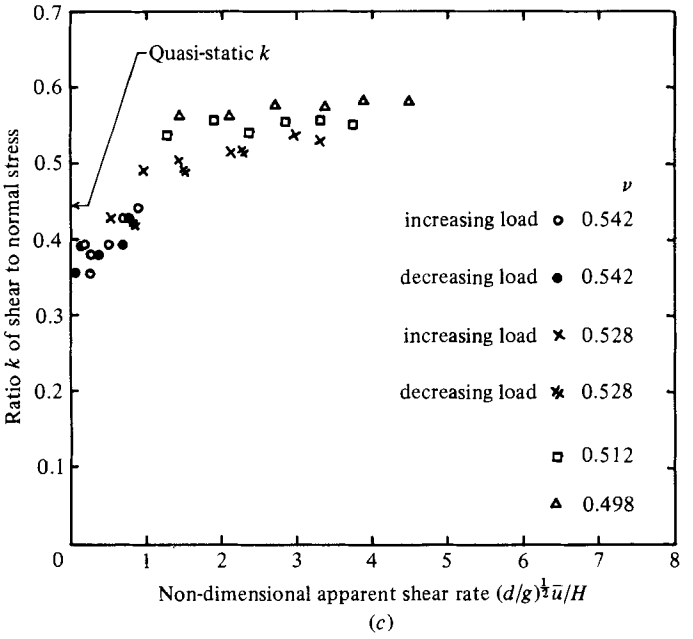

(*c*)

FIGURE 18. Experimental data for bimodal mixture of spherical polystyrene beads, material V.

different samples are no greater than those typical in the tests with the spherical particles. It is interesting to note that at the lower concentrations the non-dimensional stresses at a given non-dimensional shear rate are similar in magnitude to those measured for the spherical particles.

Both samples at the higher concentration show a type of hysteresis in which the stresses measured during unloading are greater than those measured during the loading process. As mentioned previously this may be due to a switch from a regular 'layered' shearing to a more random, disordered shear flow.

At the high concentrations the stress–shear-rate curves have sizeable regions where the slopes are less than two, indicating significant rate-independent, dry frictional contributions to the total stresses. In the high concentration data one may also observe kinks in the stress–shear-rate curves at values of nondimensional stresses of about 30–50. If one looks carefully at some of the data for the spherical particles, similar but less pronounced bends may be observed. The specific physical explanation for this behaviour, and the reasons why it occurs at *particular stress levels* or *shear rates* is not evident. However, it is worth mentioning that similar behaviour has been observed previously by Metzner & Whitlock (1958), Cheng & Richmond (1978) and Umeya (1978) during tests on concentrated suspensions.

The plots of k versus non-dimensional shear rate are shown in figures 16(*c*) and 17(*c*). Most of the values for k obtained during continued shear are *less* than the ratio of shear to normal stress measured during quasistatic yielding. This is opposite to what was observed for the spherical particles. Evidently, when compacted and sheared quasi-statically, the highly angular crushed walnut particles are effective in locking themselves together. They are thus able to develop higher shear stresses (friction angles) in this state than is possible during the collisional interactions experienced during high shear rates at lower concentrations. It may also be seen in

figures 16(*c*) and 17(*c*) that, at higher concentrations, there was a general increase in k with increasing shear rate. But at the lowest concentration, k sometimes shows a decrease with increasing shear rate similar to that observed in tests with the spherical glass particles.

4.3. *Spherical particles having a bimodal size distribution (material V)*

In order to study the effects of significantly non-uniform particle sizes, we performed tests on a binary mixture of spherical polystyrene particles; 30 % by weight of 'small' particles having a mean diameter of 0.55 mm, and 70 % by weight of 'large' particles having a diameter of 1.68 mm. The weighted mean diameter of the mixture was 1.34 mm. Data from these tests are shown in figures 18(*a–c*). The stress–shear-rate curves have slopes of less than two. This is so even for the lowest concentration of $\nu = 0.498$ that was tested. The small particles can fit in the interstices of the large ones. At high concentrations this increases the likelihood of dry frictional contributions to the total stresses over what might be expected for a monosized material. Again it is interesting to note that at low concentrations the non-dimensional stresses at a given non-dimensional shear rate (both based upon the weighted mean diameters) are similar in magnitude to those measured for the monosized spherical particles.

Although the two sizes of particles were randomly mixed when they were initially loaded into the shear cell, it was found at the end of a test, upon removal of the upper disk, that the fine particles had migrated towards the outer bottom corner of the annular trough and the coarse ones collected near the top inner corner of the trough. We can explain this size segregation physically as follows. Because of the velocity fluctuations associated with the collisional particle interactions, the interstitial voids are continuously varying in size. If the void space becomes large enough a neighbouring particle has the possibility of occupying this space. As a result of the centrifugal and gravitational forces, there is a preferred direction for particles to move if a void space becomes available. Since the sizes of the void spaces are continuously fluctuating between small and large values (their size depending upon the value of the mean concentration), the probability of the creation of a void space large enough to accept a small particle is obviously greater than the probability of the creation of a void space large enough to accept a large particle. Thus there is a net migration of fines in the direction of the resultant of the gravitational and centrifugal forces with the coarse particles being 'pushed' in the opposite direction. At low concentrations, strong secondary motions may remix the particles to some extent and the segregation is less pronounced.

Again hysteresis was observed in the stress–shear-rate curves at high concentrations. For the present tests, the stresses measured upon unloading were less than those observed during the loading phase. This might be explained in terms of the reworking or maturing process mentioned previously, but it may also be due in part to the size segregation just described. At the start of a test the particle sizes are randomly mixed. Because of centrifugal effects, the stresses acting on the upper disk assembly are non-uniform, the main contribution to the 'average' stress comes from the particles at the outer radii. As the test progresses the fines migrate to the outer radii. Since the 'dynamic' contribution to the stress depends upon the square of the particle diameter, a gradual reduction of the mean particle diameter at the outer radii could result in measured stresses at a given shear rate that were higher at the beginning of a test sequence than at the end.

The behaviour of the k versus shear-rate data was similar to that observed for the

monosized particles, an increase in k with a decrease in ν and an increase in k with increased shear rate. Except at very low shear rates, the values of k were higher than the value determined under quasi-static conditions.

5. Summary and conclusions

The present paper has described experiments performed on a number of different dry granular materials of about 1 mm in size which were sheared at high concentrations and high strain rates. The experiments made use of an annular shear cell which is the first device known to the present authors that has been designed to determine shear and normal stresses as functions of shear rate for various values of solids concentrations. The aim was to obtain viscometric data analogous to those which have been obtained previously for solids suspended in liquids. It should be emphasized that it is extremely difficult to obtain viscometric data for highly concentrated dry particles that apparently are of the same 'quality' as those which are far more easily obtained in tests with dilute suspensions. Similar difficulties have already been mentioned by Cheng & Richmond (1978) in connection with their tests of dense suspensions. They characterized their initial results as both 'chaotic' and 'anomalous', even for repeat tests with the same sample. Only after numerous tests with different materials and after careful consideration of the particulate nature of the test material did more understandable patterns begin to emerge. Our own experience during the present tests has been much the same. As a result of the annular-shear-cell data which has been gathered, correlated and interpreted, we may conclude the following.

(1) At the lower solids concentrations ($\nu \lesssim 0.5$ for the spherical glass and polystyrene and $\nu \lesssim 0.47$ for the angular crushed walnut shells) the stresses depend approximately linearly upon particle density and quadratically upon particle diameter and shear rate. This is consistent with Bagnold's (1954) simple analysis of granular flows in the *grain-inertia* regime and with more sophisticated microstructural theories in which the stresses are developed as a result of collisional momentum and energy transfer. It was also found that the test data for the different spherical materials at the lower concentrations can be collapsed reasonably well when plotted in terms of non-dimensional stress, say $\sigma/\rho_p gd$ versus non-dimensional apparent shear rate $(d/g)^{\frac{1}{2}}\,\bar{u}/H$. This kind of collapse may be somewhat fortuitous and result from compensating effects of the different material properties. For example, the granular-flow theories of Shen (1982) and Ogawa *et al.* (1980) predict the stresses to increase with increasing coefficient of restitution e and decrease with the increasing coefficient of surface friction μ. The glass beads probably had a larger e, and a higher μ, than the polystyrene beads.

(2) At higher concentrations the stresses showed significant departures from a square shear-rate dependence. In most cases the shear-rate dependence was weaker as a result of significant contributions to the stresses generated by dry frictional rubbing during enduring particle contacts. This was particularly evident for the case of the particles which had a bimodal size distribution. Frictional rubbing was no doubt enhanced since the smaller particles can fit in the interstices of the larger particles. The irregular angular crushed walnut shells also showed strong dry-friction effects. Hysteresis effects in which the stresses were different during the loading phase than the unloading phase were also observed. When the unloading stresses were *lower* than the loading stresses, the differences may be attributed to an ordering or reworking of the material as the test progressed. Other types of hysteresis observed may be related to transitions from an ordered flow in distinct layers to a more random

disordered flow involving jamming and locking together of groups of particles (*analogous* to transitions from laminar to turbulent fluid flows).

(3) The ratio k of shear stress to normal stress was not strongly dependent upon shear rate, but it increased with decreasing solids fraction ν. These trends are consistent with the constitutive behaviour which may be *inferred* from observations of granular flows down rough inclined chutes. For the spherical particles, k was generally greater than $\tan\phi$, where ϕ is the *quasi-static* internal friction angle. For the angular crushed walnut shells k was generally less than $\tan\phi$.

(4) At very high solids concentrations and small shear-gap heights, finite particle size effects were dominant. In a series of tests using spherical polystyrene beads, all at the same mean concentration of $\nu = 0.526$, the shear gap H was *varied* over a range of about one particle diameter. Values of stresses at the same shear rate were found to differ by as much as an order of magnitude. This suggests that the simple shear flow in which particles can move in distinct layers is a rather special kind of flow. Other more general flows, such as an extensional flow, or a converging or diverging flow in which the layering is less likely, would evidently develop different stresses at *high concentrations* than might be inferred from simple shear tests.

(5) Viscometric tests of dry particulates are plagued with difficulties of many kinds. It is very hard to approach the ideal of developing a relatively simple flow, avoid the many extraneous influences that can distort and complicate this simple flow and still be able to measure a sufficient number of flow-field properties from which the constitutive behaviour can be inferred. Depending upon the values of the concentration, stress levels and shear rates, it is possible for the test results to be affected in one regime or another by gravitational forces, centrifugal forces, particle segregation, secondary flows, formation of free surfaces and air gaps, the formation of locked or rigid zones, finite-particle-size phenomena, 'maturing' of individual samples during a test sequence, and transitions from 'layered' particle flows to more random motions. We have attempted to avoid these problems when possible, or to point out the likelihood of their presence and their effects upon the test results. An awareness of these effects and their complexities should be sobering to the theoretician attempting to devise continuum models to describe granular flows.

(6) There are two obvious problem areas that are in need of theoretical study. One is the boundary conditions; for example, the slip velocity at a rigid wall and its dependence upon wall roughness, the flux of particle fluctuation energy into the walls, and the possible jump in fluctuation energy there. The other problem concerns the way in which the dry-friction, rate-independent, stress contributions can be included in a rational way into some kind of theoretical framework.

The work reported here was supported by the Natural Science and Engineering Research Council of Canada (NSERC). We are indebted to W. Weaver, W. Chan and L. Toly for construction of the shear cell. W. Weaver also performed some of the exploratory experiments that were carried out prior to those reported herein. Some preliminary results of this work have been presented at the Euromech Colloquium 133 on *Statics and Dynamics of Granular Materials*, Oxford University 13–17 July 1980 and at the *18th Annual Meeting of the Society of Engineering Science*, Brown University, 2–4 September 1981.

Appendix. Effects of centrifugal forces and determination of average shear stresses

When the granular material contained in the annular shear cell is sheared during a test run both the normal and the shear stresses developed on the face of the upper disk increase with radius as a result of centrifugal effects. In the experimental arrangement the force on the torque arm attached to the upper disk assembly can be measured, and the overall torque due to the sheared granular material can be determined. To reduce these torque readings to 'average' shear stresses over the annulus, we need to know the radius at which the shear force effectively acts and hence we need some idea of the distribution of shear stress with radius. We have not measured these distributions directly and the purpose of this appendix is to *estimate* how much the exactly averaged shear stresses would differ from the values one might calculate by (2.4), which assumes that the shear stress is uniform and independent of r.

The largest difference that is possible would occur when the shear stresses are concentrated at the outer radius in the form of a spike or a delta function. For this case the shear stresses 'averaged' over the width of the trough would be given in terms of torque T as

$$\tau_s = \frac{T}{\pi R_o(R_o^2 - R_i^2)}. \tag{A 1}$$

The ratio of this shear stress to that given by (2.4), in which the shear stress is assumed constant, is

$$\frac{\tau_s}{\tau} = \frac{2}{3}\frac{(R_o^3 - R_i^3)}{R_o(R_o^2 - R_i^2)}. \tag{A 2}$$

For the present apparatus $\tau_s/\tau = 0.876$, thus the 'average' shear stress for this unrealisticly extreme stress distribution would be only 12.4% lower than that calculated by (2.4), which neglects any centrifugal effects. Thus, while we anticipate fairly small centrifugal force corrections to the 'average' shear-stress determination, it is worth going through a somewhat more detailed analysis of these effects.

We consider an element in polar cylindrical coordinates (r, θ, z) which spans the full depth of the shear gap H. For this simple analysis we *assume* that the normal stresses in the three coordinate directions are the same and equal to the depth-averaged stress σ_r.

Because of the slow secondary flows, we might anticipate a shear stress acting radially outward at the top of the element and radially inward at the bottom of the trough. Assuming that these two radial shear forces acting on the element are not only small but act to cancel each other, the equation of motion in the radial direction yields

$$\frac{\mathrm{d}\sigma_r}{\mathrm{d}r} \approx \frac{\rho \overline{u_\theta^2}}{r}, \tag{A 3}$$

where $\rho = \nu\rho_p$ is the *bulk* density, and $\overline{u_\theta^2}$ is the depth average (over the shear gap H) of the square of the circumferential velocity u_θ. Assuming that the circumferential velocity has a linear variation

$$u_\theta = \omega r\left(1 - \frac{z}{H}\right) \tag{A 4}$$

then

$$\overline{u_\theta^2} = \frac{1}{H}\int_0^H u_\theta^2 \,\mathrm{d}z = \tfrac{1}{3}\omega^2 r^2. \tag{A 5}$$

Substituting (A 5) in (A 3) and integrating yields

$$\sigma_r = \sigma_{r_i} + \tfrac{1}{6}\rho\omega^2 (r^2 - R_i^2), \tag{A 6}$$

where σ_{r_i} is the stress at the inner radius of the trough. With the assumption that the normal stresses are isotropic, we can relate σ_{r_i} to the average normal stress σ at the top disk, which is given by (2.2), thus

$$\sigma_{r_i} = \sigma - \tfrac{1}{12}\rho\omega^2 [R_o^2 - R_i^2]. \tag{A 7}$$

Now assuming that the local circumferential shear stress at the top disk is proportional to the normal stress there, we write

$$\tau_{\theta z} = k_c \sigma_z = k_c \sigma_r. \tag{A 8}$$

Then the torque given by (2.3) is

$$T = \int_{R_i}^{R_o} 2\pi r^2 k_c \sigma_r \, dr. \tag{A 9}$$

Substituting (A 6) in (A 9) we find

$$k_c = \frac{3T/\pi}{2\sigma_{r_i}(R_o^3 - R_i^3) + \rho\omega^2 [\frac{1}{5}R_o^5 - \frac{1}{3}R_o^3 R_i^2 + \frac{2}{15}R_i^5]}. \tag{A 10}$$

Neglecting centrifugal effects ($\omega \to 0$), $\sigma_{r_i} \to \sigma$ and $k_c \to k$, we obtain

$$k = \frac{3T}{2\pi\sigma(R_o^3 - R_i^3)}. \tag{A 11}$$

Using (A 7), (A 10) and (A 11), the ratio of the 'average' shear stresses over the top disk annulus accounting for centrifugal corrections to that determined by assuming the local shear stress to be uniform is

$$\frac{\tau_c}{\tau} = \frac{k_c}{k} = \left[1 + \frac{\rho\bar{u}^2}{\sigma}\beta\right]^{-1}, \tag{A 12}$$

where

$$\beta = \frac{1}{2}\left(\frac{R_o}{\bar{R}}\right)^2 \left\{ \frac{\left[\frac{1}{5} - \frac{1}{3}\left(\frac{R_i}{R_o}\right)^2 + \frac{2}{15}\left(\frac{R_i}{R_o}\right)^5\right]}{\left[1 - \left(\frac{R_i}{R_o}\right)^3\right]} - \frac{1}{6}\left[1 - \left(\frac{R_i}{R_o}\right)^2\right] \right\},$$

$$\bar{R} = \tfrac{1}{2}(R_o + R_i), \quad \bar{u} = \omega\bar{R}.$$

For the geometry of the present apparatus $\beta = 0.002470$. In terms of the non-dimensional variables used in the data presentation, (A 12) can be rewritten as

$$\frac{\tau_c}{\tau} = \left\{1 + \beta\frac{\rho_p g d}{\sigma}\nu\left(\frac{H}{d}\right)^2 \left[\left(\frac{d}{g}\right)^{\frac{1}{2}}\frac{\bar{u}}{H}\right]^2\right\}^{-1}. \tag{A 13}$$

Figure 19 shows τ_c/τ versus $(H/d)\nu^{\frac{1}{2}}[(d/g)^{\frac{1}{2}}\bar{u}/H]$ plotted for constant values of $\sigma/\rho_p g d$. For the data presented here, the centrifugal force corrections to the average shear-stress values are seen to amount to only a few percent *at most*. As the above 'corrections' are crudely estimated and are generally less than the accuracy of the experimental measurements, we have not applied them to the data. Thus all the shear-stress data presented were reduced using (2.4).

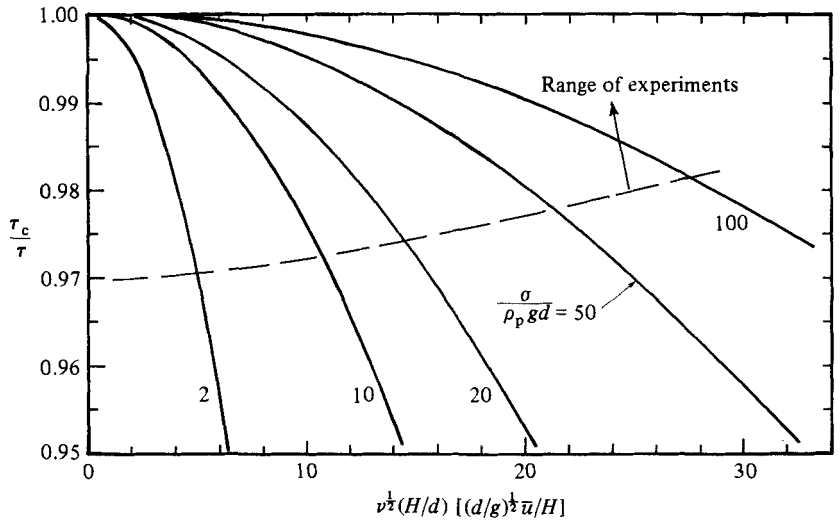

FIGURE 19. Centrifugal-force corrections for determination of average shear stress from torque measurements.

REFERENCES

ACKERMANN, N. L. & SHEN, H. H. 1982 Stresses in rapidly sheared fluid–solid mixtures. *J. Engng Mech. Div. ASCE* **108**, 95–113.

BAGNOLD, R. A. 1954 Experiments on a gravity free dispersion of large solid spheres in a Newtonian fluid under shear. *Proc. R. Soc. Lond.* A **225**, 49–63.

BAGNOLD, R. A. 1966 The shearing and dilation of dry sand and the 'singing' mechanism. *Proc. R. Soc. Lond.* A **295**, 219–232.

BRIDGWATER, J. 1972 Stress–velocity relationships for particulate solids. *ASME Paper* 72-MH-21.

CAMPBELL, C. S. & BRENNEN, C. E. 1982*a* Computer simulation of shear flows of granular materials. In *Proc. U.S.–Japan Seminar on New Models and Constitutive Relations in the Mechanics of Granular Materials* (ed. J. T. Jenkins & M. Satake). Elsevier.

CAMPBELL, C. S. & BRENNEN, C. E. 1982*b* Computer simulation of chute flows of granular materials. In *Proc. IUTAM Symp. on Deformation and Failure of Granular Materials, Delft.*

CARR, J. F. & WALKER, D. M. 1967/68 An annular shear cell for granular materials. *Powder Tech.* **1**, 369–373.

CHENG, D. C.-H. & RICHMOND, R. A. 1978 Some observations on the rheological behaviour of dense suspensions. *Rheol. Acta* **17**, 446–453.

GOLDSMITH, W. 1960 *Impact: The theory and physical behaviour of colliding solids.* Arnold.

HAWTHORNE, W. R. 1965 Engineering aspects. In *Research Frontiers in Fluid Mechanics* (ed. R. J. Seeger & G. Temple), chap. 1, pp. 1–20. Interscience.

HOFFMAN, R. L. 1972 Discontinuous and dilatant viscosity behaviour in concentrated suspensions. I. Observation of a flow instability. *Trans. Soc. Rheol.* **16**, 155–173.

HVORSLEV, M. J. 1936 A ring shearing apparatus for the determination of the shearing resistance and plastic flow of soil. In *Proc. Intl Conf. Soil Mech. Found. Engng, Cambridge, Mass.*, vol. 2, pp. 125–129.

HVORSLEV, M. J. 1939 Torsion shear tests and their place in the determination of the shearing resistance of soils. *Proc. ASTM* **39**, 999–1022.

JENKINS, J. T. & SAVAGE, S. B. 1983 A theory for the rapid flow of identical smooth, nearly elastic particles. *J. Fluid Mech.* **130**, 187–202.

MANDL, G., DE JONG, L. N. J. & MALTHA, A. 1977 Shear zones in granular material. *Rock Mech.* **9**, 95–144.

METZNER, A. B. & WHITLOCK, M. 1958 Flow behaviour of concentrated (dilatant) suspensions. *Trans. Soc. Rheol.* **2**, 239–254.

NOVOSAD, J. 1964 Apparatus for measuring the dynamic angles of internal friction and external friction of a granular material. *Collection Czech. Chem. Commun.* **29**, 2697–2701.

OGAWA, S., UMEMURA, A. & OSHIMA, N. 1980 On the equations of fully fluidized granular materials. *Z. angew. Math. Phys.* **31**, 483–493.

SAVAGE, S. B. 1978 Experiments on shear flows of cohesionless granular materials. In *Proc. U.S.–Japan Seminar on Continuum-Mechanical and Statistical Approaches in the Mechanics of Granular Materials* (ed. S. C. Cowin & M. Satake), pp. 241–54. Gakujusu Bunken Fukyu-kai.

SAVAGE, S. B. 1979 Gravity flow of cohesionless granular materials in chutes and channels. *J. Fluid Mech.* **92**, 53–96.

SAVAGE, S. B. & JEFFREY, D. J. 1981 The stress tensor in a granular flow at high shear rates. *J. Fluid Mech.* **110**, 255–272.

SCOTT, R. F. 1963 *Principles of Soil Mechanics*. Addison-Wesley.

SCARLETT, B., ACKERS, R. J., PARKINSON, J. S. & TODD, A. C. 1969/70 Application of geometrical probability to particulate systems. Part I. The critical porosity of shear granular systems. *Powder Tech.* **3**, 299–308.

SCARLETT, B. & TODD, A. C. 1968 A split ring annular shear cell for determination of the shear strength of a powder. *J. Sci. Instr.* **1**, 655–656.

SCARLETT, B. & TODD, A. C. 1969 The critical porosity of free flowing solids. *Trans. ASME* B: *J. Engng Ind.* **91**, 478–488.

SHEN, H. 1982 Constitutive relationships for fluid–solid mixtures. Ph.D. thesis, Clarkson Coll. of Tech.

STEPHENS, D. J. & BRIDGWATER, J. 1978*a* The mixing and segregation of cohesionless particulate materials. Part I. Failure zone formation. *Powder Tech.* **21**, 17–28.

STEPHENS, D. J. & BRIDGWATER, J. 1978*b* The mixing and segregation of cohesionless particulate materials. Part II. Microscopic mechanisms for particles differing in size. *Powder Tech.* **21**, 29–44.

UMEYA, K. 1978 Rheological studies on powder–liquid systems. In *Proc. U.S.–Japan Seminar on Continuum-Mechanical and Statistical Approaches in the Mechanics of Granular Materials* (ed. S. C. Cowin & M. Satake), pp. 222–240. Gakujutsu Bunken Fukyu-kai.

VOIGHT, B. (ed.) 1978 *Rockslides and Avalanches*, vol. 1. Elsevier.

VOIGHT, B. (ed.) 1979 *Rockslides and Avalanches*, vol. 2. Elsevier.